Fall 12-2022

Assembly of Ceramic Particles in Aqueous Suspensions Induced by High-Frequency AC Electric Field

James E. John IV
Old Dominion University, jj0773@gmail.com

ASSEMBLY OF CERAMIC PARTICLES IN AQUEOUS SUSPENSIONS INDUCED BY HIGH-FREQUENCY AC ELECTRIC FIELD

by

James E. John, IV
B.S. December 2019, Old Dominion University

A Thesis Submitted to the Faculty of
Old Dominion University in Partial Fulfillment of the
Requirements for the Degree of

MASTER OF SCIENCE

MECHANICAL ENGINEERING

OLD DOMINION UNIVERSITY
December 2022

Approved by:

Dipankar Ghosh (Director)

Sebastian Bawab (Member)

Hamid Eisazadeh (Member)

ABSTRACT

ASSEMBLY OF CERAMIC PARTICLES IN AQUEOUS SUSPENSIONS INDUCED BY HIGH-FREQUENCY AC ELECTRIC FIELD

James E. John, IV
Old Dominion University, 2022
Director: Dr. Dipankar Ghosh

Ceramic materials processed using colloidal methods have been the focus of a great deal of research aimed at tailoring the final structure and microstructure of the finished ceramic sample. To this end, various external field effects have been investigated to modify the suspension microstructure without manipulating the ceramic particles directly. In a previous work in the field of ice templating it has been shown that AC electric fields are able to produce microstructural changes in ice templated ceramics that have significantly improved the final mechanical properties. However, the mechanisms for this process are still not well understood in ceramics.

To better understand the mechanisms that are present in colloidal processing of ceramics using AC field, this thesis investigates the role of high frequency alternating current (AC) electric field in the assembly of alumina and barium titanate particles in aqueous media. Field-particle interactions were *in situ* investigated via optical microscope for coarse and fine alumina as well as fine barium titanate powder particles in very dilute suspensions. In the first half of the work with both coarse and fine alumina particles, AC field-induced assembly led to the formation of chains aligned in the field direction. Chain length increased with both field strength and field duration. Chain formation was attributed to mutual dielectrophoretic (DEP) interaction forces. Threshold field strength for chain formation suggested stronger interactions for finer particles.

In the second half of the work, fine alumina and fine barium titanate powders of similar size were compared to study the effect of the particle type on the formation of chains. The inter-

chain distance was also measured suggesting that the particle type had a strong effect on how the chain structure developed. The effect of frequency on chain formation showed that decreasing the frequency of the AC field resulted in fluid motion that impeded the formation of chains. Darvan-C dispersant was added to the medium of the solution improving the formation of chains for both alumina and barium titanate. SEM images were used to confirm these findings by preserving the chains using a binder.

ACKNOWLEDGEMENTS

I would like to thank my advisor and committee for their help and support. I would especially like to express my sincere gratitude to Dr. Ghosh for his help and guidance in my research. I am grateful for all the help he gave in completing my first paper and the research in this thesis. His knowledge and expertise were a great benefit in my understanding of academic research, and his constant motivation was greatly beneficial to me. I would also like to thank Dr. Bawab for his part in helping me to complete my master's degree and thesis and he and Dr. Eisazadeh for being a part of my committee.

I also would like to give my appreciation to the colleagues that I shared this journey with, both during my time as an undergrad and as a graduate student in Dr. Ghosh's laboratory. I would like to especially thank Sashanka Akurati, Mahesh Banda, and Rohan Parai for teaching me everything I needed to know to be successful during my undergraduate research.

Lastly, I would like to thank my family and friends who have supported and encouraged me.

NOMENCLATURE

V_A	Van der Walls energy
V_B	Repulsive Electrostatic Double Layer Force
r	Particle radius
$\tilde{E}$	Electric field
$K_i(\omega)$	Claussius- Mossotti factor
$\mathrm{Re}\lvert K\rvert$	Real part of Claussius- Mossotti factor
ε_p^*	Complex permittivity of particle
ε_m^*	Complex permittivity of medium
ε_p	Permittivity of particle
ε_m	Permittivity of medium
σ_p	Conductivity of particle
σ_m	Conductivity of medium
f	Frequency of AC electric field
ω	Angular frequency
F_{dep}	Dielectrophoretic force
F_{chains}	Chaining Force

Table of Contents

LIST OF TABLES

LIST OF FIGURES

Figure Page

Figure Page

Figure Page

Figure Page

CHAPTER 1

1 INTRODUCTION

1.1 Colloidal Processing of Ceramics

Ceramic materials are subject to extensive research as they offer many distinct advantages over polymers or metals including superior hardness, chemical inertness and low fracture toughness that are essential to many applications including sharp edged tools, filters, sensors, capacitors, and actuators [1].

Ceramic materials have traditionally been fabricated by fusion or sintering of complex mixtures in powder form. The powder processing techniques of ceramics begin with the synthesizing of powder, followed by using a mold or vessel to mold the powder into the desired shape and size. [2] The ‘green body’ is sintered at high temperature to fuse the powder into a solid structure which gives the ceramic its final microstructure and properties. Defects in the ceramic microstructure that arise from the powder processing result in stress concentration points and cracks that grow under stress and become fracture origins leading to a crack propagation and failure in the material below the expected material limits [2].

Higher quality ceramics with fine grains and minimal porosity require fine powders and uniform high-density packing. The reduction of inhomogeneity in microstructure and defects with better control over inter-particle interaction to produce dense green bodies, is possible by dispersed suspensions through colloidal processing [3]. Colloidal processing works by dispersing fine ceramic particles in the nanometer to micrometer range in a fluid media. The suspension can then be used with other processes such as casting, gel forming, and ice-templating. To make the colloidal suspension stable anionic and cationic dispersants are often used to change the pH of the

suspension. Stability of the suspension is determined by interactions between the attractive van der Waals force (VA) and repulsive electrostatic double layer force (VB). [3]

Ice-templating, also called freeze casting, is a method for processing ceramics that involves colloidal processing of ceramic powders to form a unidirectional porous structure [4,5,6]. The technique, shown in Fig.1.1 starts with a slurry containing solvent primary phase and a templated secondary phase. The solvent can be any liquid so long as it can be directionally frozen rejecting the secondary phase and then sublimated; however, water is the most common liquid used due to its convenience and the resulting structure of the ice crystal growth. The secondary phase can be from any family of materials so long as it is able to be dispersed evenly throughout the solvent and rejected during the templating process [5,6]. The resulting suspension combining the solute and the solvent along with any other additives should be a stable colloidal suspension. Once the suspension has been mixed, generally with a dispersant and soluble binder, the suspensions are unidirectionally solidified. In order to uni-directionally solidify the suspension, the suspensions are generally poured into a Teflon mold and placed on a metal “Cold-finger” which is exposed to a cold source such as liquid nitrogen. The complete assembly is radially insulated to prevent radial freezing and to keep ice-nucleation only near the cold finger region. Once freezing begins the ice-crystals grow along the unidirectional temperature gradient, and the ceramic particles are either rejected or entrapped within the ice crystals [4,5,6]. Ceramic particles rejected from the growing ice crystals are forced into alternate layers of packed ceramic particles between the ice crystals oriented along the temperature gradient as seen below inFig. 1.1b. Once the solvent has been sublimated out, only the secondary phase remains with pores formed from the removal of the ice crystals, seen in Fig. 1.1c. [4,5,6] The benefits of this process over other techniques for processing porous ceramics comes from its ease, simplicity, and flexibility [4].

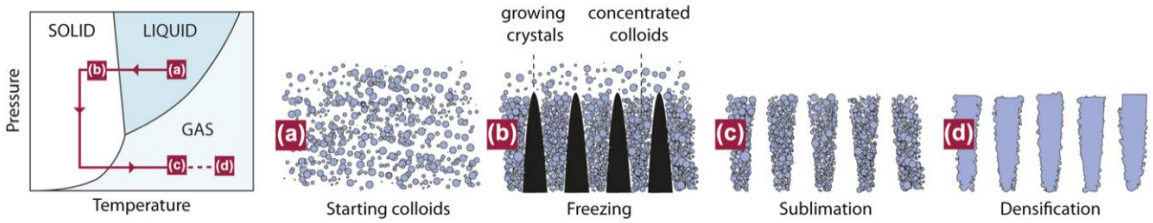

Fig. 1.1 Schematic diagram of the ice-templating showing the phase progression of water starting with colloids (a). Then the freezing processes and particle rejection (b) and then sublimation (c) and sintering (d)[5]

1.2 Colloidal Processing and Ice-Templating with Fields

Manipulation and assembly of ceramic particles in an aqueous media using externally energized fields are of great interest because of their fundamental and practical significance in colloidal processing. Assembly of colloidal particles is governed by the local interactions between the particles and the underlying mechanism which strongly depend both on specific properties of individual particles and their surrounding medium. [7,8] One method that has been shown to be able to influence the motion of particles in colloidal processing is the use of magnetic fields. In these experiments a magnetic field is used to exert a torque on a magnetic particle to align the particle with anisotropic geometry or magnetic properties along the field direction. [9,10] In non-uniform magnetic fields, the field gradient enables particle motion. [9,10] Since advanced ceramics such as alumina (Al_2O_3), zirconia (ZrO_2), barium titanate ($BaTiO_3$), and titania (TiO_2) are weakly or nonmagnetic, ferrimagnetic iron oxide (Fe_3O_4) nanoparticles are used to surface magnetize these ceramics to respond to the applied magnetic field. [9] In one study, a static magnetic field was used in conjunction with ice-templating to influence the microstructure of titania (TiO_2) porous ceramics. [9] The magnetic field with a field strength of 0.12 T was applied perpendicular to the growth direction of ice crystals. The application of the magnetic field resulted in the alignment of

lamella walls on the plane perpendicular to growth direction in the resultant titania porous scaffolds. During mechanical testing the ice-templated ceramics fabricated using magnetic fields exhibited a two-fold increase in compressive strength in the transverse direction (perpendicular to growth direction) compared to the ones ice-templated without field. [10] In Fig. 1.2 a-c mold designs are shown for the application of magnetic fields on colloidal suspensions during ice templating. In Fig. 1.2 d-f the field lines are shown that corresponded with the ceramic microstructure after freezing.

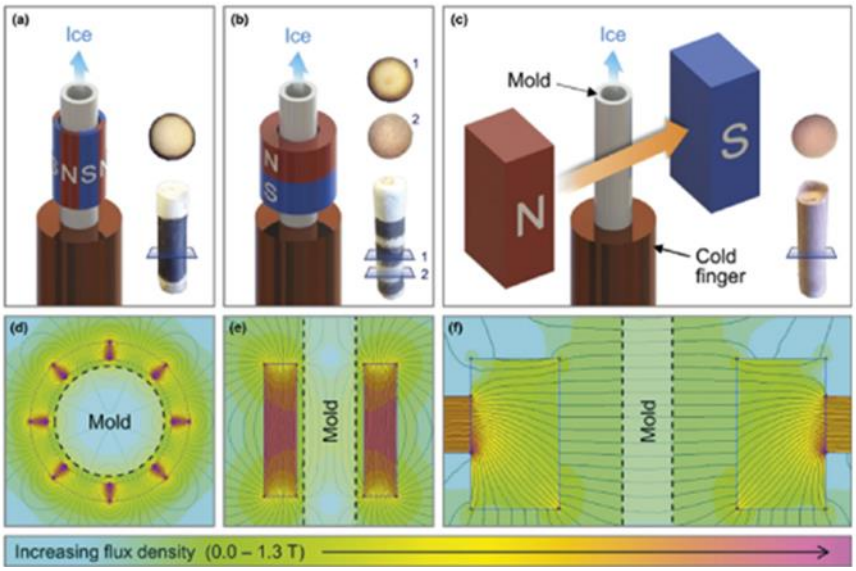

Fig. 1.2 a-c ice-templating setups to apply magnetic fields. d-f schematic of magnetic field lines for ice templating molds with magnetic field setups. [10]

Another method for influencing colloidal processing using external fields that has been tested is the use of acoustic fields. In these tests mechanical input forces are used to externally create fields created using acoustic pressure waves. The acoustic pressure waves enable the manipulation of particle position and orientation within suspensions and have been used to create

dense porous ring-like structures and ripple effects, Fig. 1.3. [11, 12] However, achieving acoustic orientation and positioning is extremely difficult in suspensions with ceramic volume fraction above 10%. [11]

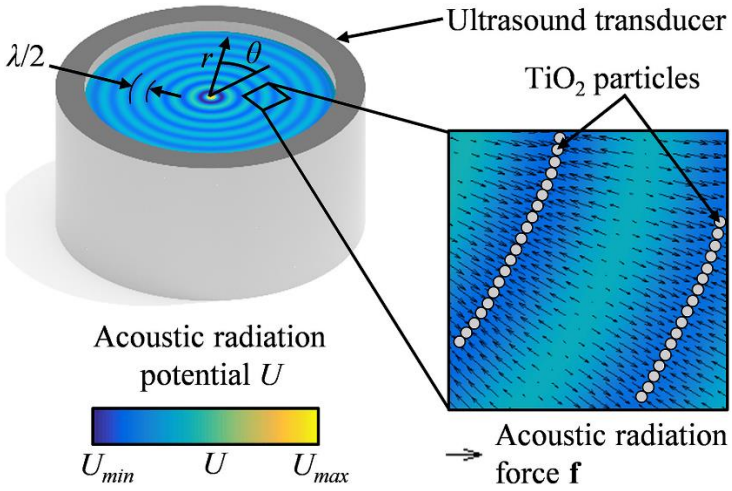

Fig. 1.3 Acoustic radiation within a cylindrical ultrasound transducer showing particles aggregated in a concentric pattern. [11]

DC current has been experimented with as a method for influencing colloidal processing as well. [13,14] In colloidal processing, DC fields have been shown to be able to rotate and align particles with the field direction, as well as move them along the field direction. DC field application has been used to create bi-layered ceramic structures such that there is a dense secondary layer at the bottom of the ice-templated structure. [13] DC fields applied were also applied perpendicular to the direction of the applied temperature gradient. The walls in ice-templated alumina (Al_2O_3) were aligned along the field direction, and compressive strength increased in that direction. [13]

The application of AC field has also been experimented with in freeze casting with promising results, but so far there has been very little work in the area, and its mechanisms are not yet fully understood. However, AC field and dielectrophoresis have been used in the fields of biomedical research extensively. [15]

1.3 Dielectrophoresis

Application of an alternating current (AC) electric field to a media containing particles with electrical properties (permittivity and conductivity) different than the media results in electric field non-uniformity. [15,16,17,18] The particles in the media experience frequency-dependent polarization, and the interactions of the induced diploes in the particles with the non-uniform electric field result in the dielectrophoretic (DEP) forces, which induce particle motion and inter-particle interactions. Particles experience DEP force in a non-uniform electric field only, and the force does not depend on the field polarity. [15] AC electric fields can be created and controlled at large spatial scales. Contrary to magnetically-driven assembly of particles where specific magnetic properties of colloids and solvent are required, the only necessary requirement for AC field-induced inter-particle interactions is a contrast between complex dielectric permittivity of the particle and solvent. [15, 16] Another major advantage is that the AC dielectrophoresis can be used to exploit the frequency-dependent dielectric properties of particles to control manipulation forces. Due to the long-range nature of dipolar interactions, the assembly of particles using AC fields can be realized over a large area. While the DEP forces have been used for the manipulation of polymeric particles, live cells, DNA, and carbon nanotubes (CNTs), such studies are sparse for advanced ceramic material particles in aqueous media. [15, 16, 17, 18] However, manipulation of

ceramic particles in aqueous media via the DEP forces is particularly of interest because of its fundamental and practical relevance to colloidal ceramic processing.

A mathematical model for the dielectric forces can be described using an AC electric field applied with a frequency of ω across a suspension containing dielectric particles; it causes temporary polarization within the particles. The induced dipoles in the particles interact with the gradient in the applied AC field creating a localized non-uniform field which results in dielectrophoretic (DEP) forces. [13, 19] The time-averaged DEP force on each particle, F_{DEP}, depend on the gradient of the field squared ($\nabla\widetilde{\mathrm{E}}^2$) and the radius cubed of the particle (r^3, effective volume). Since the DEP force on a particle are proportional to the gradient of the field squared, F_{DEP} does not change its sign during the field oscillations and attains a nonzero time-average value. F_{DEP} is expressed as [20,21,22]

$$F_{\mathrm{DEP}} = 2\pi\varepsilon_{\mathrm{m}}\mathrm{Re}|K(\omega)|r^3\nabla\left|\widetilde{\mathrm{E}}\right|^2, \quad (1)$$

where $\mathrm{Re}|K|$ is the real part of the dipolar Clausius-Mossotti factor (CMF) that embodies the frequency-dependent dielectric properties of the particle and its surroundings which give rise to the induced dipole moment. *K* is expressed as [20, 21, and 22]

$$K = \frac{\varepsilon_{\mathrm{p}}^* - \varepsilon_{\mathrm{m}}^*}{\varepsilon_{\mathrm{p}}^* + 2\varepsilon_{\mathrm{m}}^*}. \quad (2)$$

$\varepsilon_{\mathrm{p}}^*$ and $\varepsilon_{\mathrm{m}}^*$ are the complex permittivities of the particle and medium, respectively. $\varepsilon_{\mathrm{p}}^*$ is expressed as [20,21,22]

$$\varepsilon_{\mathrm{p}}^* = \varepsilon_{\mathrm{p}} - j\frac{\sigma_{\mathrm{p}}}{\omega}, \quad (3)$$

whereas $\varepsilon_{\mathrm{m}}^*$ is expressed as [20, 21, 22]

$$\varepsilon_{\mathrm{m}}^* = \varepsilon_{\mathrm{m}} - j\frac{\sigma_{\mathrm{m}}}{\omega}. \quad (4)$$

ε_{m} and σ_{m} are the absolute dielectric permittivity and electrical conductivity of the medium, respectively. ε_{p} and σ_{p} are the absolute dielectric permittivity and electrical conductivity of the particles, respectively. The relative polarizability of the particle in the medium depends on the real part of CMF. The non-uniform AC field induces a mutual DEP interaction force for each particle, and the magnitude of the interaction force increases with the decreasing distance between particles. [23, 24, 25] If the mutual DEP force is attractive, particles approach each other and form a chain. [23, 24, 25] The "chaining force" F_{chains} depends on the field strength squared ($\widetilde{\mathrm{E}}^2$) and the radius squared of the particle (r^2). F_{chains} is expressed as: [13,19]

$$F_{\mathrm{chains}} = -C\pi\varepsilon_{\mathrm{m}} r^2 K^2 \left|\widetilde{\mathrm{E}}\right|^2. \qquad (5)$$

1.4 Motivation for Current Work

In previous work by Akurati et al. [23], 26 vol% aqueous Al_2O_3 suspensions were prepared by mixing ceramic powder with deionized (DI) water containing 1 wt.% (of ceramic powder) anionic dispersant ammonium polymethacrylate. The mixture was then ball milled for 24 hours and then sieved and de-aired. The electrode connected to the power amplifier terminal supplying the AC signal from the function generator is referred to as the source electrode (S), and the electrode receiving the signal from the source electrode and transmitting it back to the power amplifier and oscilloscope is referred to as the reference electrode (R) in Fig. 1.4. [26]

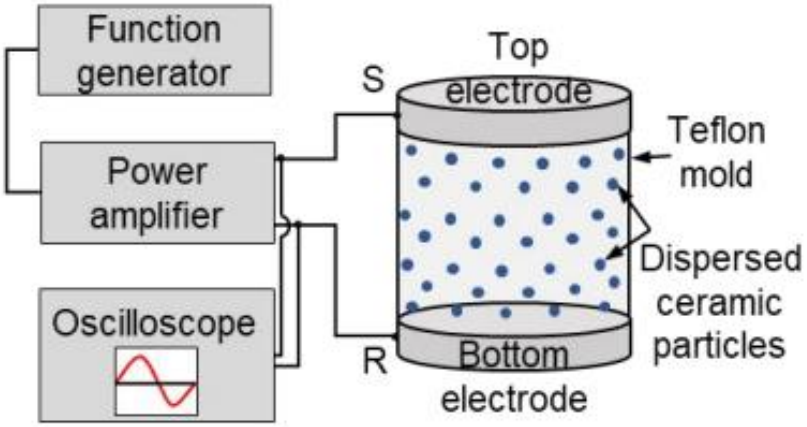

Fig. 1.4 Schematic representation of experimental setup for AC field application to aqueous ceramic suspension. [26]

In this work the electric field conditions of 1 kHz to 1 MHz were used with a maximum voltage of approximately 200 V peak-to-peak. It was found that 250 to 500 kHz had the largest effect on the microstructure of the suspension and the sintered ceramic. In the sintered ceramic there was an increased concentration of particles in suspension near the cold-finger which resulted in the development of finer ice crystals compared to those without the field. [26] The uniaxial compressive response (stress-strain curves) was taken for control samples (no field) in Fig. 1.5a, and for t of 3, 5 and 10 minutes in Fig. 1.5b-d. [26] From these it was shown that compared to control samples, samples exposed to AC electric field exhibited significantly greater strength. [26] The samples exposed to AC field between 3 and 5 minutes exhibited 3- to 4-times higher σ_m compared to the control samples. However, beyond 5 minutes, materials exhibited a decrease of σ_m but still had higher strength than control samples. Beyond this work there is, however, a lack of understanding as to the mechanisms and tunability of AC field interactions with ice-templated

ceramics. To fill this gap in understanding this work aims to investigate this AC phenomena to better understand its mechanisms and interactions with various factors present in ice-templating.

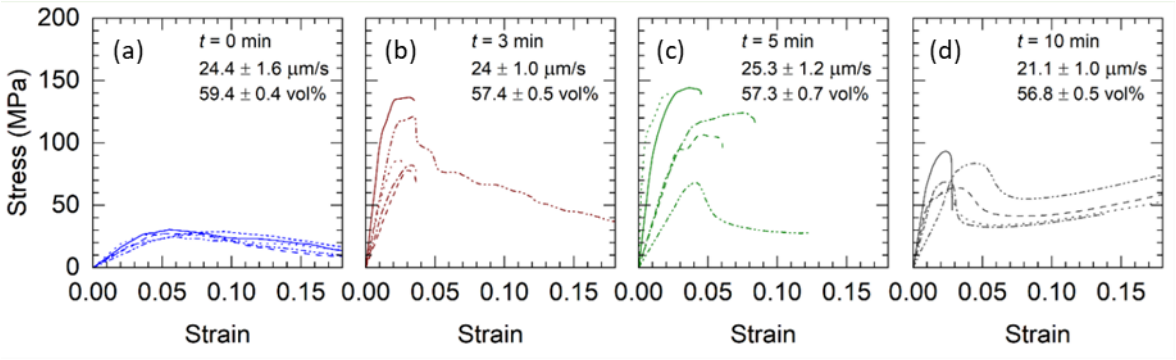

Fig. 1.5 Uniaxial compressive stress strain curves of materials fabricated (a) without and (b-d) with field (t of 3, 5 and 10 minutes). [26]

In the previous work the final structure of the ice templated materials was investigated, but there is a gap in the research in understanding the mechanisms and particle motions that created the final structure. While previous studies have described the motion of biological particles in AC dielectrophoresis the motion of ceramic particles has not been captured in images or video for analysis. Being able to view the path and motion of the particles in a video and image form is key to understanding how they form their final structures. By viewing the motion of particles in a video as well as viewing an image and observing the change in the variables, including the field conditions as well as the particle and media properties, we can better learn how to tailor the particle motion. In the previous work it was shown that the voltage, frequency, and time of applied field showed an effect on the final ceramic microstructure. However, it is unclear how these variables contribute to the final structure. Additionally, in the previous research only one particle type and size were tested, and all samples were made with anionic dispersant in the suspension.

To fill the gaps in the previous research in the following work we *in situ* investigated assembly of Al_2O_3 and $BaTiO_3$ particles based on the factors of size distribution and particle type as they were subject to high-frequency AC field. Fine alumina particles of d_{50} = 0.40 μm and coarse alumina particles of d_{50} = 2.72 were chosen to study the particle size effect since particle radius affects the strength of the dielectric forces on the particle. [20, 21, 22] The coarse particles were initially chosen since they were small enough to be dispersed easily in suspension and large enough to easily see under the optical microscope. The finer size particles were chosen due to them being approximately one magnitude smaller than the large particles while still being visible under the optical microscope. Dilute aqueous suspensions were prepared for the various particle types so that the particles would be easily visible under the optical microscope allowing their motion and inter-particle interactions due to the application of AC field to be recorded. If the suspension was too concentrated, the suspension would be too opaque for particle motion to be viewed through the optical microscope. AC field was applied through two identical coplanar, parallel metal electrodes, which created a spatially homogeneous electric field perpendicular to the two metal electrodes in the absence of particles. [13,19] With the addition of the particles the uniform electric field was distorted by the changes in conductivity and permittivity causing a non-uniform electric field. The conductivity and permittivity of the particles relative to the suspension impacts the dielectric forces on the particles as mentioned in equations 1-5. Therefore, it was important for us to investigate two different particle types with significantly different electrical properties. Since alumina has relatively low conductivity and permittivity with 1x10-12 S/m and 9.2 ε0, respectively barium titanate was chosen to represent particles with higher dielectric properties since it has a conductivity of 1 x 10-7 S/m and permittivity of 6500 ε0. [27, 28, 29, 30] The inter-particle

interactions were investigated as a function of the applied AC field strength, duration, and frequency similar to the previous work involving ice templating. The stability of the field-induced assembly of particles was also studied to assess how the suspension microstructure might be impacted by removal of the field as well as the effect of adding anionic dispersant ammonium polymethacrylate (Darvan-C, R.T. Vanderbilt Co, Norwalk, CT) since dispersant is required to achieve a fully dispersed suspension. Finally, DEP behavior of particles was investigated using dissimilar size electrodes, which created a spatially non-uniform electric field to investigate the directionality of the dep forces.

CHAPTER 2

2 ASSEMBLY OF ALUMINA PARTICLES IN AQUEOUS SUSPENSIONS INDUCED BY HIGH-FREQUENCY AC ELECTRIC FIELD

Note: The contents of this chapter have been published in the Journal of American Ceramic Society

John, JE, Qian, S, Ghosh, D Assembly of alumina particles in aqueous suspensions induced high frequency AC electric field. J Am Ceram Soc. 2022; 105: 5598– 5610.

https://doi.org/10.1111/jace.18527

2.1 Introduction

Manipulation and assembly of ceramic particles in an aqueous media using externally energized fields are of great interest because of their fundamental and practical significance in colloidal processing. Assembly of colloidal particles is governed by the local interactions between particles and the underlying mechanism strongly depends both on specific properties of individual particles and their surrounding medium. [7,8] A magnetic field exerts a torque on a magnetic particle that aligns the particle with anisotropic geometry or magnetic properties along the field direction. [9] In non-uniform magnetic fields, the field gradient enables particle motion. [7,8,9,10] Since advanced ceramics such as alumina (Al_2O_3), zirconia (ZrO_2), barium titanate ($BaTiO_3$), and titania (TiO_2) are weakly or nonmagnetic, ferrimagnetic iron oxide (Fe_3O_4) nanoparticles are used to surface magnetize these ceramics to respond to the applied magnetic field.[8] Mechanical external fields created by acoustic pressure waves also enable the manipulation of particle position and orientation. [7, 8, 11, 12] However, achieving acoustic orientation and positioning is extremely difficult in suspensions with ceramic volume fraction above 10%. [7]

Application of an alternating current (AC) electric field to a media containing particles with electrical properties (permittivity and conductivity) different than the media results in electric field non-uniformity. [14,15] The particles in the media experience frequency-dependent polarization, and the interactions of the induced dipoles in the particles with the non-uniform electric field result in the dielectrophoretic (DEP) forces, which induce particle motion and inter-particle interactions. Particles experience DEP force in a non-uniform electric field only and the force does not depend on the field polarity. AC electric fields can be created and controlled at large spatial scales. Contrary to magnetically driven assembly of particles where specific magnetic properties of colloids and solvent are required, the only necessary requirement for AC field-induced inter-particle interactions is a contrast between complex dielectric permittivity of the particle and solvent. [9, 10, 14, 15, 16] Another major advantage is that the AC dielectrophoresis can be used to exploit the frequency-dependent dielectric properties of particles to control manipulation forces. Due to the long-range nature of dipolar interactions, the assembly of particles using AC fields can be realized over a large area. While the DEP forces have been used for the manipulation of polymeric particles, live cells, DNA, and carbon nanotubes (CNTs), [15, 16, 17, 18] such studies are sparse for advanced ceramic material particles in aqueous media. However, manipulation of ceramic particles in aqueous media via the DEP forces is particularly of interest because of its fundamental and practical relevance to colloidal ceramic processing.

This work *in situ* investigated assembly of Al_2O_3 particles with board size distribution induced through local, attractive inter-particle interactions in aqueous media subject to high-frequency AC field. The interactions were studied for very dilute aqueous suspensions prepared from coarse and fine Al_2O_3 particles. The purpose of using very dilute suspension was to enable visualization of individual particles and their motion to study inter-particle interactions due to the

AC electrical field using an optical microscope whereas the purpose of using two Al_2O_3 powders of very different particle size was to study the size effects on the interactions. The AC electrical field was applied through two identical coplanar, parallel metal electrodes, which created a spatially homogeneous electric field perpendicular to the two metal electrodes in the absence of particles. However, a spatially non-uniform electric field was induced by the suspending particles. The inter-particle interactions were investigated as a function of the applied AC field strength and duration, and the stability of the field-induced assembly of particles was also studied. Finally, DEP behavior of Al_2O_3 particles was investigated using dissimilar size electrodes, which created a spatially non-uniform electric field. The current research findings provide insights into the interactions between high-frequency AC electric field and ceramic particles in aqueous media for particle motion and assembly, which can potentially enable the fabrication of novel ceramic patterns and structures via the colloidal processing route employing AC electric fields.

2.2 Experimental Procedure

Very dilute (0.02 vol.%) aqueous ceramic suspensions were prepared by mixing alfa-Al_2O_3 powder particles and deionized (DI) water. For each suspension, powder and DI water in the required quantities were taken in a glass beaker and mixed using a magnetic stirrer. Two Al_2O_3 powders with very different particle sizes were used in this work, which were purchased. The powders were used in the as-received form. One set of suspensions were prepared from coarse Al_2O_3 powder (referred to as CA, purchased from Sigma-Aldrich, Saint Louis, MO), whereas another set of suspensions were prepared from fine Al_2O_3 powder (referred to as FA, purchased from Inframat Advanced Materials, Amherst, NY). Both Sigma-Aldrich and Inframat Advanced Materials are very reliable sources for ceramic powders. Scanning electron microscope (SEM)

images of CA and FA powders are shown in Fig. 2.1a and 1b, respectively. The size of the individual particles was measured from the SEM images. For this purpose, 0.5 g of powder was added to 80 ml of DI water and the mixture was sonicated for 10 minutes. A drop of the suspension was placed on carbon tape which covered a SEM stud, which was then placed in an oven at 120 °C to dry the tape. Next, SEM images were taken, and the images were processed using open-source image processing software Fiji - ImageJ® (NIH, USA) to enhance sharpness and contrast. Fig. S1a and 1b (Supplementary Information) show an SEM image of FA powder before and after image processing, respectively. "Trainable Weka Segmentation (TWS)" plugin available in Fiji - ImageJ® was then used to separate the powder from the background, Fig. S1c. The powder size was then determined using the "particle analysis" plugin in Fiji - ImageJ®. For CA powder, a total of 900 particles were measured. Similarly, for FA powder, a total of 750 particles were measured. Based on these measurements, both particle size distribution and cumulative distribution of CA and FA powders are shown in Fig. 2.1e and 1f, respectively. CA powder exhibited a wide and very asymmetric distribution of particle size, whereas FA powder exhibited relatively symmetric distribution of particle size. In the figures, d_{10}, d_{50} and d_{90} values are indicated. d_{10} represents that 10% of the particles are smaller than the value indicated by the vertical arrow. d_{50} represents that 50% of the particles are smaller than the value indicated by the vertical arrow. Finally, d_{90} represents that 90% of the particles are smaller than the value indicated by the vertical arrow. For CA particles, estimated d_{10}, d_{50} and d_{90} values were 0.51, 2.72 and 6.55 μm, respectively. For FA particles, estimated d_{10}, d_{50} and d_{90} values were 0.06, 0.4 and 0.63 μm, respectively. Clearly, particle size was much finer in FA powder than in CA powder, whose d_{50} was about one order higher than that of FA powder. Therefore, due to the wide particle size difference, the selection of CA and FA powders allowed for the study of particle size effects on the inter-particle interactions

and particle assembly. This particle size range is also relevant in aqueous suspension-based processing of ceramics. [31]

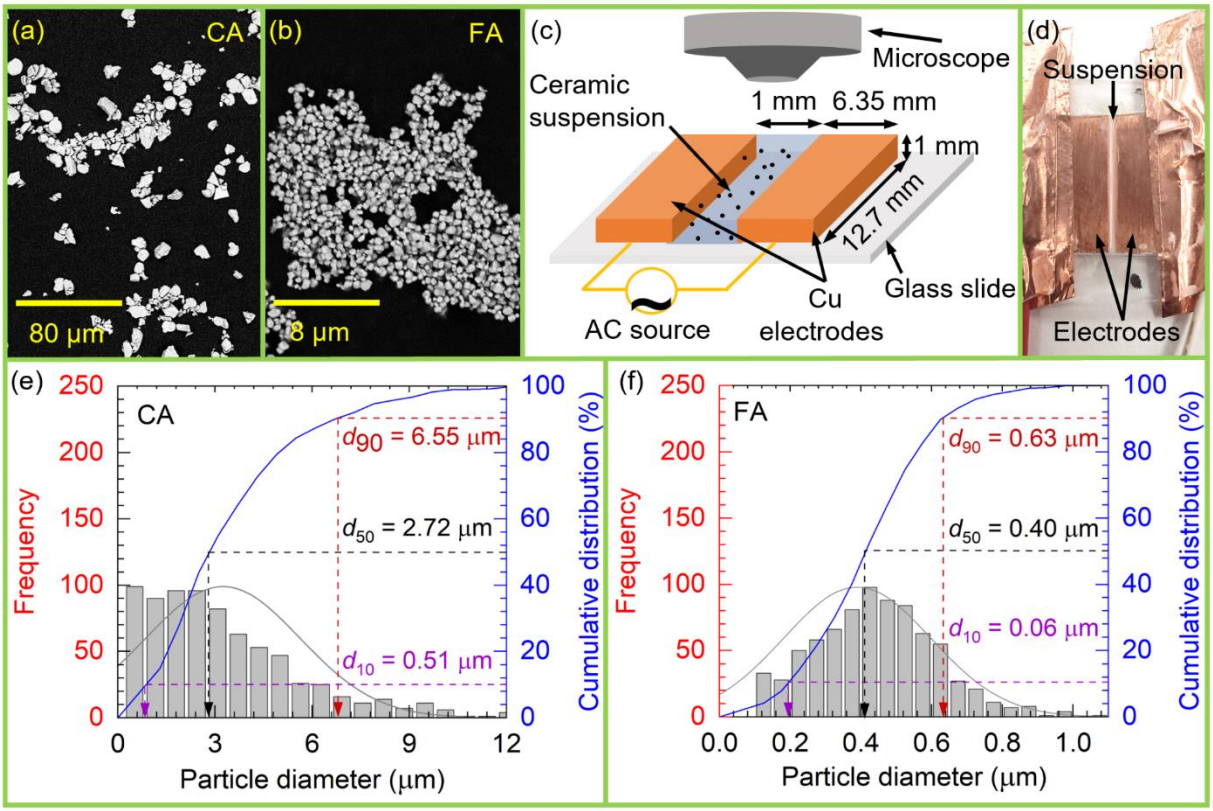

Fig. 2.1 Scanning electron microscope (SEM) image of (a) coarse alumina (CA) and (b) fine alumina (FA) powder particles. (c) Schematic of experimental setup (not to scale). (d) Optical image of the actual setup with ceramic suspension present between Cu electrodes. Particle size distribution and cumulative distribution in (e) CA powder and (f) FA powder

Fig. 2.1c shows a schematic of the experimental setup, which consisted of two identical coplanar, parallel copper (Cu) electrodes attached to a glass slide. Cu electrodes were of rectangular shape with 1 mm thickness and the gap between the electrodes was 1 mm. A function

generator (Tektronix AFG 3102) and a voltage amplifier (Tegam model 2340) were used to apply an AC electrical field, whereas voltages across the electrodes during the experiments were monitored through an oscilloscope (Tektronix TDS 1002). For each experiment, the gap between Cu electrodes was filled with Al_2O_3 suspension and the suspension height was about 1 mm. Each experiment was *in situ* observed and recorded using an optical microscope (Leica DM6 M, Buffalo Grove, IL). An image of the Cu electrodes with Al_2O_3 suspension placed between the electrodes is shown in Fig. 2.1d. In the experiments to study chain formation, AC electrical fields were applied at 1 MHz for a maximum duration (t) of 120 seconds. The use of high AC frequency avoided any electrolysis in water.

In the first set of experiments, the applied peak-to-peak AC voltage (V_{pp}) was systematically changed to vary field strength (V/mm) and find the threshold value for each powder, where the threshold field strength was determined as the critical field strength where formation of particle–particle chains occurred through particle assembly. While below the threshold field strength particle motion was observed, chain formation did not occur. For both CA and FA suspensions, a series of studies were performed at various field strengths. Note that for both powders, experimental results are reported for the threshold field strength and for the field strengths above that. However, the maximum field strength achieved (200 V/mm) was limited by the highest AC voltage that can be applied via the function generator and voltage amplifier used in this work. Since the gap between two electrodes was fixed (1 mm), field strength was varied by changing the applied V_{pp}. From the analyses of the videos of the experiments (recorded at 60 fps.) using the Leica optical microscope, the effects of particle size, field strength and field duration on inter-particle interactions and chain formation were quantified in terms of chain length and inter-

chain distance. For each field strength and powder type, two experiments were performed to assess reproducibility.

Another set of experiments were performed to study the stability of the chains which formed in the suspensions due to the AC field. These experiments were performed at a particular field strength using identical coplanar, parallel Cu electrodes. In these experiments, an electrical field was applied for different durations (1, 3, 5 and 7 minutes) and suspensions were imaged before field application and after field application for the desired duration while having the field still ON, and 1 minute after the field was removed.

Finally, DEP behavior of CA and FA particles was investigated to determine whether the particles exhibited negative-DEP (n-DEP) or positive-DEP (p-DEP) behavior at the frequency where the experiments were performed. Under p-DEP, particles move towards the regions of higher field strength, whereas n-DEP corresponds to the behavior of particles moving towards the regions of lower field strength. To study DEP behavior, Cu electrodes of dissimilar size were used to deliberately apply a spatially non-uniform AC field to aqueous Al_2O_3 suspensions, and migration of particles in the suspensions were observed using an optical microscope (Leica DM6 M, Buffalo Grove, IL).

2.3 Results and Discussion

2.3.1 Assembly in aqueous suspensions containing coarse alumina particles

Fig. 2.2 shows optical images (a-i) revealing *in situ* inter-particle interactions, assembly, and pattern formation in CA suspensions subject to high-frequency (1 MHz) AC field at representative field strengths of 50 V/mm, 100 V/mm, and 180 V/mm. Electrodes were on the left-hand and right-hand sides of the images. 50 V/mm was found to be the threshold field strength.

Below this field strength, while particle motion was observed, chain formation did not occur. In this section, qualitative discussion is presented based on the observations from the optical microscope images, whereas quantitative analysis of chain length and inter-chain distance estimated from the images is presented in Section 3.3. Chain formation due to inter-particle interactions occurred within 30 seconds of the electrical field application and chain length increased with field duration. At 50 V/mm, considerable displacement of particles occurred within the first 15 seconds during which many particles moved close to each other. Inter-particle interactions resulted in the formation of small chains containing a few particles each aligned in the direction of the applied field, as indicated by the blue dashed ellipses in Fig. 2.2b. By 30 seconds (Fig. 2.2c), more chains had formed with a likely increase in chain length. However, isolated particles can still be observed at several locations. Fig. 2.2e and f suggest a relative increase in inter-particle interactions at 100 V/mm, which is based on the increase in chain length (discussed further in Section 3.3). Furthermore, at 180 V/mm, much longer chains developed within 15 seconds (Fig. 2.2h), and chain length continued to increase by 30 seconds (Fig. 2.2i). Therefore, based on the qualitative observations from the optical images, it can be concluded that inter-particle interactions increased with field strength, which led to greater assembly and increased chain length.

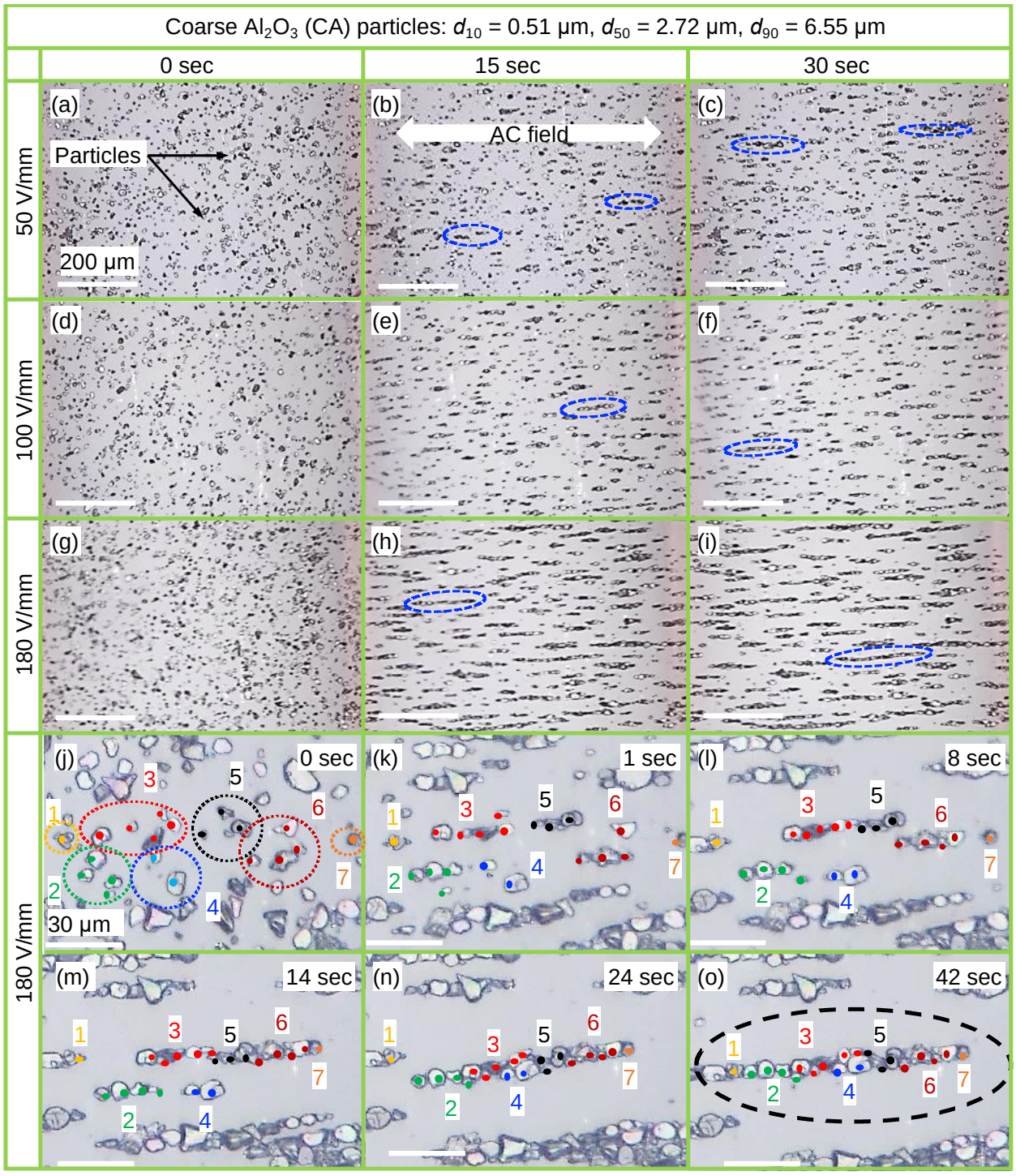

Fig. 2.2 Optical microscope images revealing inter-particle interaction in CA suspensions subject to 1 MHz AC field at representative field strengths of 50 V/mm (a–c), 100 V/mm (d–f), and 180 V/mm (g–i). In (a–i), images in the left column show distribution of particles prior to AC

field application. Images in the middle column and right column show assembly and chain formation after 15 and 30 s of field application, respectively. (j–o) A series of higher magnification optical microscope images revealing particle motion and the process of a single chain formation over 42 s at 180 V/mm

More details of the mechanism of particle assembly and chain formation in the CA suspension are revealed through a series of higher magnification optical images in Fig. 2.2j-o at 180 V/mm field strength. Using time-resolved information, displacements of some of the particles were tracked, starting from their initial (mostly) isolated positions before the application of field, to their ending positions in particle chains. For example, in Fig. 2.2j (before field application), a few individual and groups of particles were identified using different colors, dashed circles, and numbers (1-7). When the field was turned ON, an instantaneous change occurred, Fig. 2.2k (1 second). Within the individual groups of particles, displacement of particles occurred, resulting in the particles moving closer to each other and developing small chains, aligned along the field direction. By 14 seconds (Fig. 2.2m), some of the small chains (3, 5, 6) joined to form a longer chain. As the field duration increased, the process continued. By 42 seconds, all the identified groups of particles (1-7) combined to form a single long chain. Thus, a two-step process was involved in inter-particle interactions and particle assembly. First, immediately after turning the field ON, the displacements of the nearby individual particles toward each other led to the formation of small chains containing only a few particles, which were oriented along the direction of the field. Next, as the field duration increased, small chains developed interconnections, resulting in the formation of longer chains. One such a long chain is indicated by a dashed ellipse in Fig. 2.2o. The kinetics of inter-particle interactions and chain formation were fast and required

less than 1 min. Similar observations were made for several chains, which all revealed the same process of chain formation. Thus, images in Fig. 2.2j-o truly represent the mechanism of chain formation due to AC field.

2.3.2 Assembly in aqueous suspensions containing fine alumina particles

For FA suspensions, optical images at three representative field strengths of 28 V/mm, 100 V/mm, and 180 V/mm are shown in Fig. 2.3a-i. In this section, qualitative discussion is presented based on the observations from the optical microscope images, whereas quantitative analysis of chain length and inter-chain distance estimated from the images is presented in Section 3.3. Compared to CA particles, threshold field strength for FA particles was lower, 24 V/mm compared to 50 V/mm, which is unexpected since the DEP force is proportional to the volume of the particles. Note that the presence of particles in a media creates a spatially non-uniform electric field due to the perturbation of the field by the particles. For the same ceramic volume fraction, FA suspension contained more particles than CA suspensions leading to smaller inter-particle distance. The presence of more particles with smaller particle distance created higher local non-uniform electric field around each particle and consequently generated DEP forces of higher magnitude. Therefore, the threshold field strength to form particle chains was lower in FA suspension than that in CA suspension. Fig. 2.3a-i revealed markedly enhanced inter-particle interactions in FA suspensions, suggesting a strong influence of particle size on AC field-induced inter-particle interactions and assembly in aqueous ceramic suspensions. At comparable field strengths, it appears that longer chains and more of them formed in FA suspensions within 15 seconds (Fig. 2.3b, e, h), and chain length increased by 30 seconds (Fig. 2.3c, f, i). At higher field strengths, it appears that several chains were spanning almost over the entire length between two electrodes (Fig. 2.3f, i). Higher

magnification images in Fig. 2.3j-o revealed that the mechanism of particle assembly and chain formation in FA suspensions were similar to that observed in CA suspensions. Fig. 2.3o shows the formation of a long chain in the suspension.

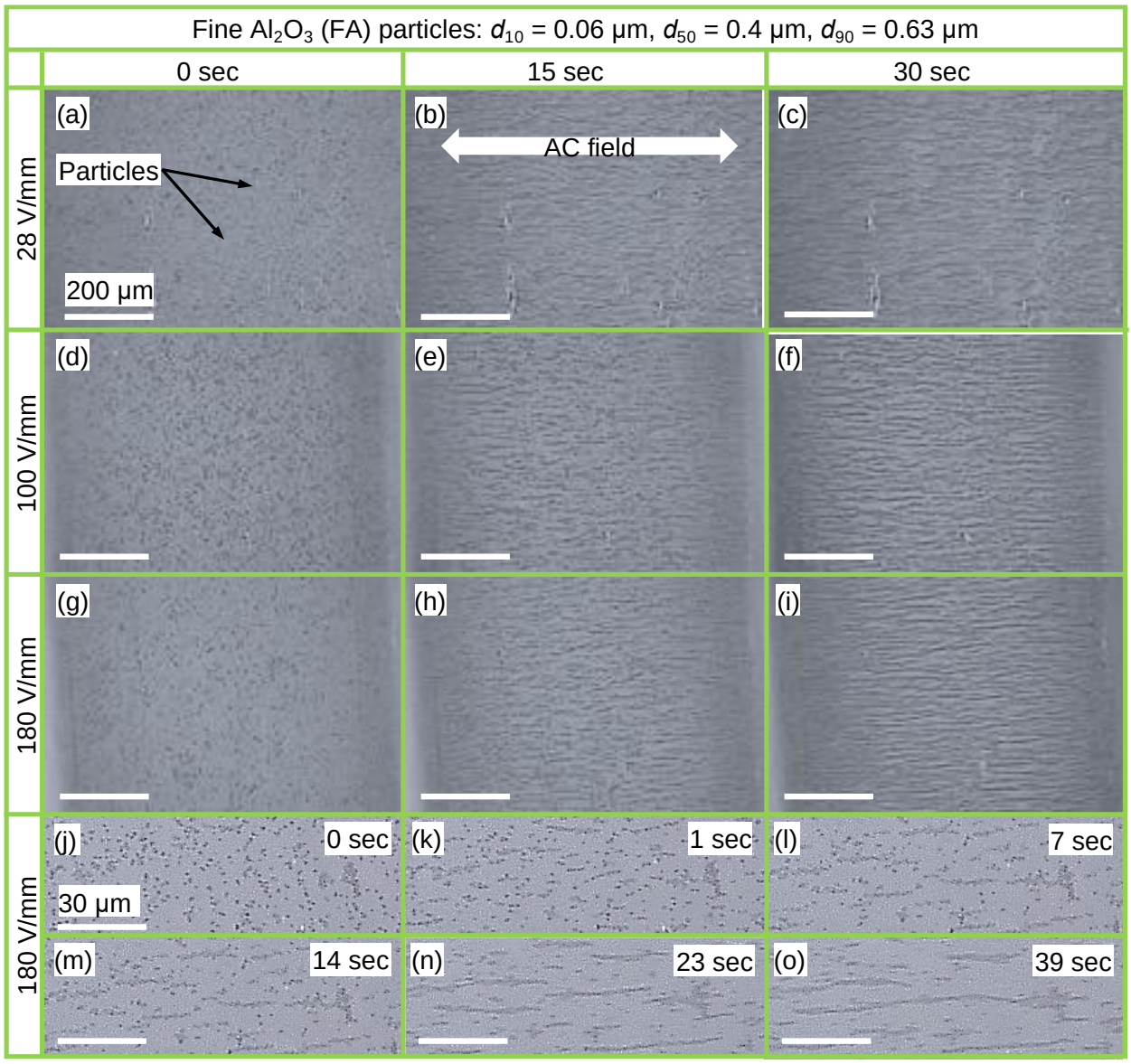

Fig. 2.3 Optical microscope images revealing inter-particle interaction in FA suspensions subject to 1 MHz AC field at representative field strengths of 28 V/mm (a–c), 100 V/mm (d–f), and 180 V/mm (g–i). In (a–i), images in the left column show distribution of particles prior to field

application. Images in the middle column and right column show assembly and chain formation after 15 and 30 s of field application, respectively. (j–o) A series of higher magnification optical microscope images revealing the mechanism of assembly and chain formation over 39 s at 180 V/mm.

2.3.3 Chain length and inter-chain distance

The current results revealed a marked difference in the "suspension microstructure" between CA and FA suspensions with an extensive network of particle chains evolved in the FA suspensions. Thus, at the same field strength, a much finer microstructure evolved in the FA suspension compared to the CA suspension. Differences between suspension microstructures were quantified from image analysis in terms of chain length and inter-chain distance. Fig. 2.4a and b shows average chain length evolution with field duration in CA and FA suspensions, respectively, at various field strengths. Standard deviation chain length increased with field strength. In CA suspensions, at any given duration, chain length increased consistently with field strength. At each field strength, chain length also increased with field duration. At 200 V/mm, the maximum chain length was observed to be about 90 μm when the field duration was 120 seconds. Taking d_{50} 2.72 μm as average particle size, about 33 CA particles were estimated to be present in a chain of length 90 μm. For FA suspensions, chain length also increased with field strength and duration. However, compared to CA particles, FA particles exhibited a greater increase in chain length with field duration. Also, at higher field durations, chain length was higher in FA suspensions than in CA suspensions. Chain length in FA suspensions reached as high as 120 μm at 200 V/mm at the field duration of 120 seconds. Taking d_{50} = 0.4 μm as average particle size, about 300 FA particles were

estimated to be present in a chain of length 120 μm. Thus, a much larger number of particles interacted to develop each individual chain in FA suspensions.

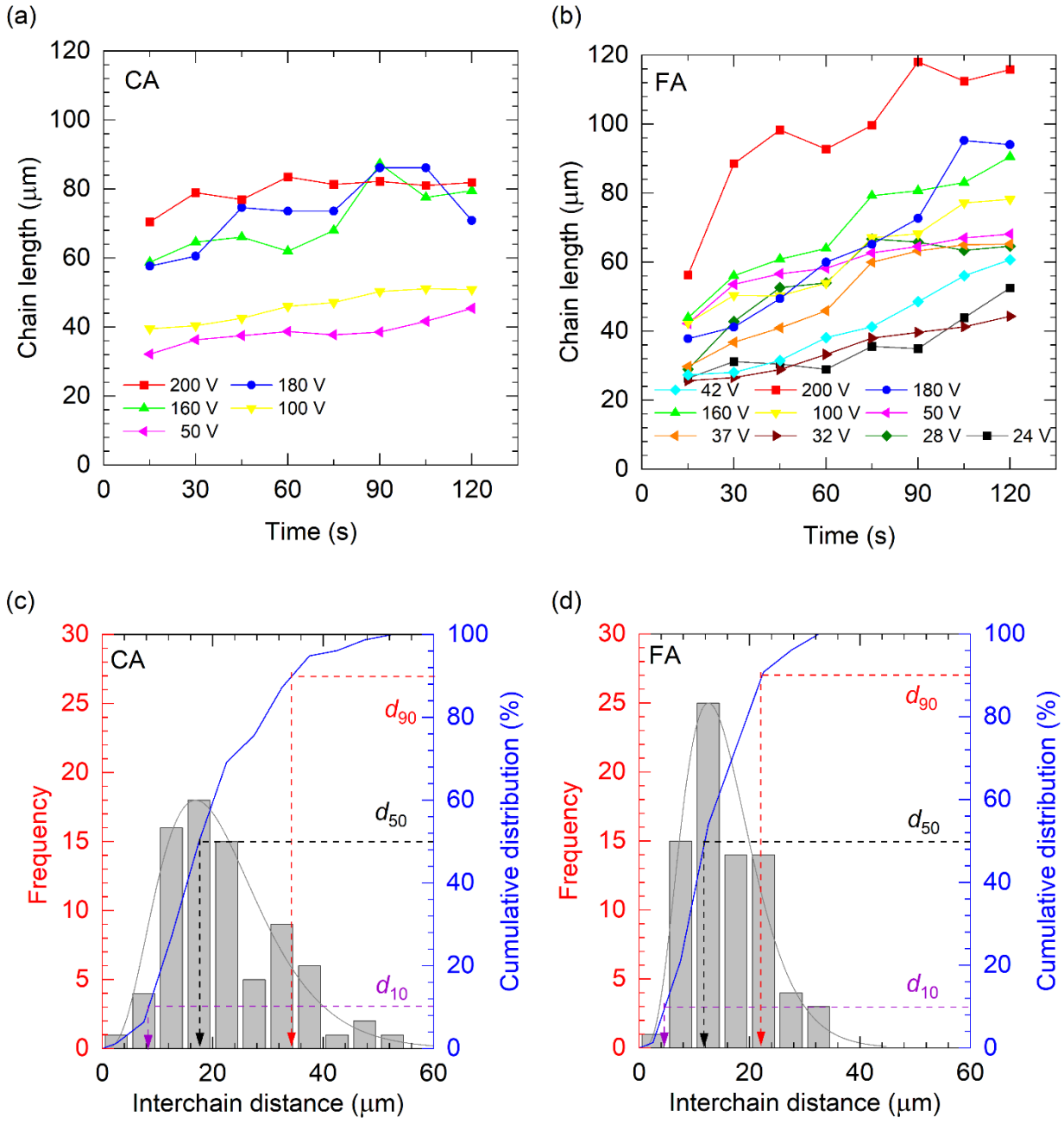

Fig. 2.4 Variation in chain length with field duration in (a) CA and (b) FA suspensions at various field strengths. The distribution and cumulative distribution of inter-chain distances perpendicular to the field direction after 30 s at 180 V/mm for (c) CA and (d) FA suspensions

Fig. 2.4c and d shows distribution of inter-chain distances (measured perpendicular to field direction between two adjacent chains) and cumulative distribution in CA and FA suspensions, respectively, at 30 seconds for the field strength of 180 V/mm. Inter-chain distance distribution was relatively symmetric in FA suspension compared to CA suspension, suggesting a relatively homogeneous suspension microstructure in the former suspension. This behavior is attributed to a narrower particle size distribution in FA powder than in the CA powder, as shown in Fig. 2.1e and 1f. For CA suspension, d_{10}, d_{50} and d_{90} values for inter-chain distances were 8.4, 17.5 and 34.3 μm, respectively. For FA suspension, d_{10}, d_{50} and d_{90} values for inter-chain distances were 4.7, 11.9 and 22.3 μm, respectively. Quantitative image analysis thus reinforced that at the same field strength, a much finer microstructure evolved in FA suspension than in CA suspension, attesting to the influence of particle size on the AC field-induced ceramic suspension microstructure.

Chain formation of Al_2O_3 particles in aqueous suspensions is attributed to the DEP forces. Due to the AC dielectrophoresis, formation of particle chains is a known phenomenon, which has been studied both experimentally and numerically for various materials, such as polystyrene particles and CNTs. [32, 33] As a result, AC dielectrophoresis has emerged as a potential mechanism for particle manipulation and positioning in a media. However, as was mentioned previously, such studies are lacking for advanced ceramic material particles in aqueous media, creating a knowledge gap, which was the motivation for this current study. In the following, the origin of DEP forces and chain formation are briefly discussed.

An AC electric field applied with a frequency of ω across a suspension containing dielectric particles causes temporary polarization of the particles. The induced dipoles in the particles interact with the gradient in the applied AC field, giving rise to dielectrophoretic (DEP)

forces. [13,19] Non-uniform field is a requirement to generate DEP forces. The time-averaged DEP force on each particle, F_{DEP}, depends on the gradient of the field squared ($\nabla\widetilde{\mathrm{E}}^2$) and the radius cubed of the particle (r^3, effective volume). Since the DEP force on a particle is proportional to the gradient of the field squared, F_{DEP} does not change its sign during the field oscillations and attains a nonzero time-average value. F_{DEP} is expressed as [20,21,22]

$$F_{\mathrm{DEP}} = 2\pi\varepsilon_{\mathrm{m}}\mathrm{Re}|K(\omega)|r^3\nabla\left|\widetilde{\mathrm{E}}\right|^2, \quad (1)$$

where $\mathrm{Re}|K|$ is the real part of the dipolar Clausius-Mossotti factor (CMF) that embodies the frequency-dependent dielectric properties of the particle and its surroundings which give rise to the induced dipole moment. *K* expressed as [20, 21, and 22]

$$K = \frac{\varepsilon_{\mathrm{p}}^* - \varepsilon_{\mathrm{m}}^*}{\varepsilon_{\mathrm{p}}^* + 2\varepsilon_{\mathrm{m}}^*}. \quad (2)$$

Here, $\varepsilon_{\mathrm{p}}^*$ and $\varepsilon_{\mathrm{m}}^*$ are the complex permittivities of the particle and medium, respectively. $\varepsilon_{\mathrm{p}}^*$ is expressed as [20,21,22]

$$\varepsilon_{\mathrm{p}}^* = \varepsilon_{\mathrm{p}} - j\frac{\sigma_{\mathrm{p}}}{\omega}, \quad (3)$$

whereas $\varepsilon_{\mathrm{m}}^*$ is expressed as [20,21,22]

$$\varepsilon_{\mathrm{m}}^* = \varepsilon_{\mathrm{m}} - j\frac{\sigma_{\mathrm{m}}}{\omega}. \quad (4)$$

Here ε_{m} and σ_{m} are the absolute dielectric permittivity and electrical conductivity of the medium, respectively. ε_{p} and σ_{p} are the absolute dielectric permittivity and electrical conductivity of the particles, respectively. The relative polarizability of the particle in the medium depends on the real part of CMF. Although AC field in this work was applied through two identical coplanar, parallel electrodes, the field around particles was spatially non-uniform due to the perturbation of the field by the particles. [18,22,23] The non-uniform AC field induces a mutual DEP interaction force for each particle, and the magnitude of the interaction force increases with the decreasing distance

between particles. [24,25] If the mutual DEP force is attractive, particles approach each other and form a chain. [23, 24, 25] The "chaining force" F_{chains} depends on the field strength squared ($\widetilde{\text{E}}^2$) and the radius squared of the particle (r^2). F_{chains} is expressed as: [13,19]

$$F_{\text{chains}} = -C\pi\varepsilon_{\text{m}} r^2 K^2 \left|\widetilde{\text{E}}\right|^2. \quad (5)$$

Therefore, as suggested by equation (5), the increase in chain length with field strength for both CA and FA suspensions could be attributed to the increase in the magnitude of F_{chains} with field strength.

Equation (5) suggests that the magnitude of F_{chains} will also increase with particle size. Distortion of the electric field increases with the increasing diameter of particles.[21, 22] Current results revealed that chain length was not significantly different between the CA and FA suspensions at most of the field strengths; however, at very high field strengths applied for 2 minutes, chain length was higher in FA suspensions than in CA suspensions. Additionally, an extensive network of particle chains evolved in FA suspensions, and suspension microstructure was much finer than in the CA suspensions. This unexpected result is attributed to the increase in inter-particle distance with particle size. For the same particle volume fraction, with the increasing particle size, the number of particles present in suspension decreases and inter-particle distance increases. This is evident from Figs. 2.2a and 2.3a, where clearly inter-particle distance was higher in the CA suspension than in the FA suspension. Therefore, while equation (5) suggests that the magnitude of F_{chains} would increase with particle size, the increase in inter-particle distance could offset that effect owing to less perturbation of the electric field. Instead, with the decreasing particle size and thus inter-particle distance, mutual DEP attractive interactions between particles can become more favorable. With the decreasing particle size, as the number of particles within a

unit suspension volume increase, more particles would be available for mutual interactions leading to a finer suspension microstructure, as was the case in FA suspensions.

2.3.4 Stability of particle assembly

Fig. 2.5a-i shows optical images of the FA suspension microstructure for application of field at 50 V/mm and field was applied for 1, 3, 5 and 7 minutes. Optical images in the left column (a, d, g, j) show the distribution of particles prior to field application. Optical images in the middle column (b, e, h, k) were captured after field application while the field was still ON, whereas the images in the right column (c, f, i, l) were captured 1 minute after the field was removed. The purpose was to reveal whether suspension microstructure could be retained after field removal and the effects of applied AC field duration on pattern formation and stability. Prior to field application, particles were randomly oriented in DI water. Clearly, the field duration had a marked influence on assembly and chain formation with a pattern well developed by 3 minutes (Fig. 2.5e) and chain length increased with field duration. Therefore, a well-developed pattern in suspension can be achieved even at lower field strength provided the field is extended for a longer duration. Fig. 2.5 revealed that the suspension microstructure which developed due to the field was disrupted as soon as the field was removed. Lower field duration was associated with a weak pattern stability resulting in the particles completely dispersing once the field was removed. Correspondingly, higher field duration was associated with an improved pattern stability and retention following the field removal. Thus, field duration seems to have an impact on pattern stability.

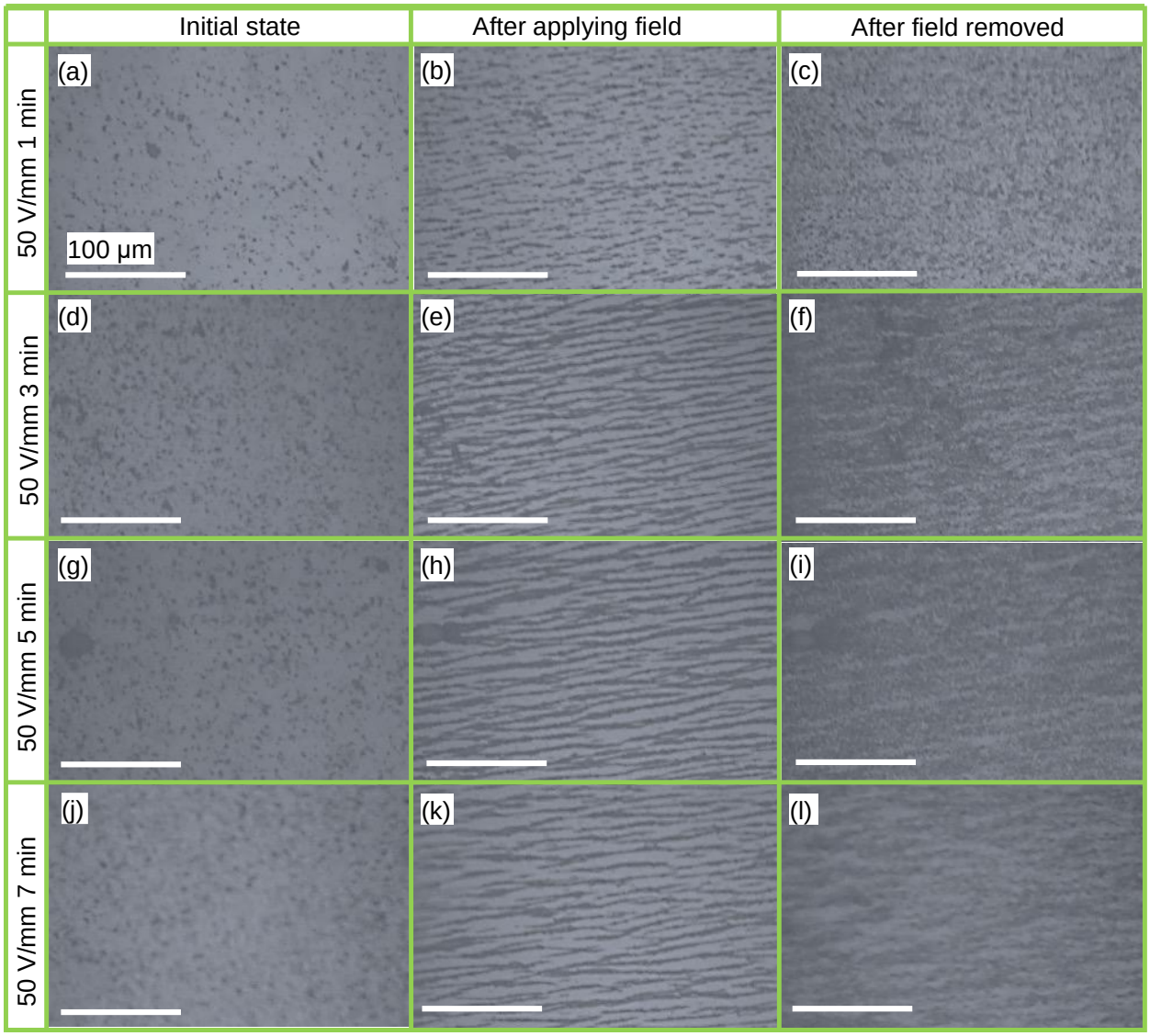

Fig. 2.5 Optical images of FA suspension microstructure (a, d, g, j) before the application of AC electric field, (b, e, h, k) after application of field for different duration (1, 3, 5, and 7 min) while the field was still ON, and (c, f, i, l) 1 min after the field was removed at a field strength of 50 V/mm

One of the observations from Fig. 2.5b was that after 1 minute of field, considerable displacement occurred where individual particles were drawn out from the pockets of

agglomerates into small to moderately sized chains. Following the removal of the field after 1 minute, suspension microstructure was disrupted, but particles were more uniformly dispersed, as seen in Fig. 2.5c, than prior to field application. After applying the field for 3 minutes (Fig. 2.5e) the increase in field duration caused an increase in the inter-particle interactions resulting in longer and a more well-defined pattern of chains. The increase in inter-particle interactions resulted in more stable chain structures and the pattern was retained to some extent after the field was removed (Fig. 2.5f). Furthermore, as the field duration increased to 5 and 7 minutes (Fig. 2.5h and k), the inter-chain interactions led to adjacent chains joining to form thicker chains. Consequently, following the removal of the AC field, the thicker chains with larger inter-chain distances retained their structure better relative to those with fewer inter-particle and inter-chain interactions. Therefore, it is concluded that inter-particle and inter-chain interactions increased with the AC field duration which resulted in a better pattern stability and retention after the removal of the field.

While not shown here, for the CA suspensions, no disruption in AC field-induced suspension microstructure was observed after field removal. It is possible that due to the much larger size, CA particles were unable to move by themselves and as a result, pattern was completely retained. Thus, pattern stability also depended on particle size.

2.3.5 Particle motion in non-uniform AC field

The experiments described in the previous sections revealed the influence of field strength and duration on assembly and chain formation in aqueous ceramic suspensions. In these experiments, AC field was applied via two identical coplanar, parallel electrodes, and chain formation occurred for both CA and FA particles. However, for further insights into the mechanism of chain formation, it is important to understand whether Al_2O_3 particles moved toward

the regions of stronger field strength (i.e., p-DEP) or weaker field strength (i.e., n-DEP). While mutual DEP interaction forces resulted in assembly and chain formation, particle size variation could result in different mechanisms for chain formation. To identify n-DEP and p-DEP, it was thus required to deliberately apply non-uniform AC field and study particle motion.

Whether a particle would exhibit n-DEP or p-DEP behavior at a frequency depends on the sign of CMF, where CMF is positive and negative for p-DEP and n-DEP, respectively. From equations (2 – 4), magnitude and sign of CMF depends on the electrical properties (permittivity and conductivity) of the particles and the media as well as the frequency of the applied field. The frequency at which the CMF shifts between positive value and negative value is called the crossover frequency. MyDEP software [21] was used to calculate CMF variation with AC field frequency over the range of 100 Hz to 2 MHz for aqueous Al_2O_3 suspension. CMF calculation was based on equations (2 – 4). Electrical conductivity and relative permittivity of bulk Al_2O_3 were taken as $1x10^{-12}$ S/m and 9.2, respectively. [30,31] Relative permittivity of DI water was taken as 80.1, whereas electrical conductivity of DI water was experimentally determined to be $2.5x10^{-6}$ S/m measured using a conductivity meter (HI2255, HANNA Instruments, Smithfield, RI).

Fig. 2.6a shows that CMF was negative over the entire frequency range, although with the increasing frequency, the magnitude of CMF decreased. Thus, in non-uniform AC field, Al_2O_3 particles would exhibit n-DEP behavior and move toward the regions of weaker field strength. However, in addition to frequency, CMF depends on particle size [22] and the calculation of CMF using bulk properties did not consider particle size effects on the electrical properties. Therefore, it was necessary to experimentally determine whether CA and FA particles would move in the same or opposite direction in a non-uniform AC field at 1 MHz when the previously described experiments were performed.

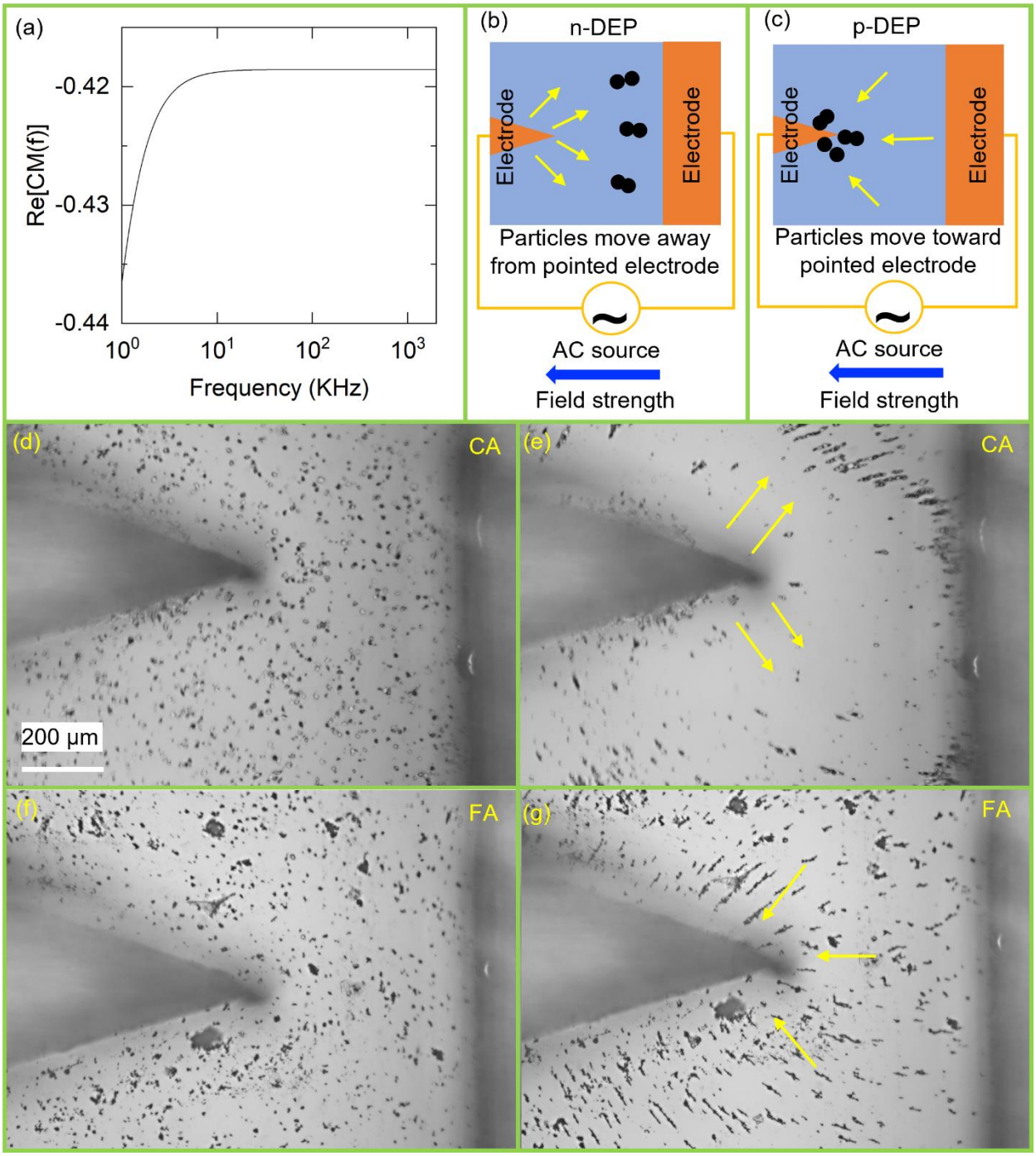

Fig. 2.6 (a) Variation in CMF with frequency calculated based on conductivity and permittivity of bulk alumina and deionized water. Illustrative schematic of particle motion for (b) n-DEP and (c) p-DEP behavior of particles in non-uniform AC field. n-DEP particles would move toward the plate electrode, that is, toward the regions of weaker field strength (b), whereas p-DEP

particles would migrate toward the pointed electrode, that is, toward the regions of stronger field strength (c). Application of field on (d–e) CA and (f–g) FA suspensions over 60 s revealed n-DEP behavior for CA particles and p-DEP behavior for FA particles

Fig. 2.6b and c schematically illustrate n-DEP and p-DEP behavior of particles, respectively, where the setup consists of a triangular pointed electrode (left) and a rectangular plate electrode (right) attached to a glass slide. Both electrodes were coplanar and the gap between the sharp end of the triangular electrode and the plate electrode was approximately 700 μm. Application of AC field through this electrode configuration creates a highly non-uniform field strength distribution between the electrodes, with the field strength being strongest in the vicinity of the sharp end of the triangular electrode and weakest in the vicinity of the plate electrode. For n-DEP behavior, particles would move toward the plate electrode, i.e., toward the regions of weaker field strength as shown in Fig. 2.6b whereas the particles would migrate toward the pointed electrode for p-DEP behavior, i.e., toward the regions of stronger field strength. Fig. 2.6c. Fig. 2.6d and e show the distribution of CA particles before and after field application for 60 seconds at 1 MHz, respectively. Similarly, Fig. 2.6f and g show the distribution of FA particles before and after field application for 60 seconds at 1 MHz, respectively. For CA particles, when the field was turned on, the particles were rapidly pushed away from the pointed electrode and migrated toward the plate electrode. Thus, Fig. 2.6e revealed that CA particles experienced n-DEP behavior at 1 MHz, which was consistent with the CMF calculations shown in Fig. 2.6a. On the other hand, when AC electric field was applied to FA particles, the particles migrated to the pointed electrode (Fig. 2.6g), which suggested p-DEP behavior at 1 MHz. Thus, while CMF calculations based on bulk properties predicted the DEP behavior for larger ceramic particles, the prediction was not

accurate for very fine particles since surface conductance of a particle changes with its surface area. As a result, *in situ* investigations were important to experimentally observe particle motion and determine DEP behavior.

Based on the above experiments, it was concluded that in the experiments where AC field was applied through two identical coplanar plate electrodes, CA particles and FA particles exhibited n-DEP and p-DEP behavior, respectively. Although both CA and FA particles formed chains when AC field was applied via two identical electrodes, the electric field distribution arising from the mutual particle-particle interaction was expected to be different, yielding different mechanisms of chain formation (one was due to n-DEP and the other was due to p-DEP). For CA particles, field strength was weaker in the region between the particles, and the particles moved toward regions of weaker field strength (n-DEP) and formed chains. For FA particles, field strength was stronger in the region between the particles, and the particles moved toward regions of stronger field strength (p-DEP) and formed chains. Under mutual DEP interaction force, both p-DEP and n-DEP ceramic particles formed particle chains in the direction parallel to the applied electric field.

The current results on the interactions between ceramic particles in aqueous media and external AC electric field are invaluable to realize the full potential of the AC dielectrophoresis in ceramic processing for particle motion, spatial redistribution, and assembly in the synthesis of novel ceramic materials and structures. The current studies were intentionally conducted for very dilute suspensions, which enabled the visual recording of particle motion and pattern formation using an optical microscope. While it would be very challenging to visualize particle motion in concentrated ceramic suspensions, which are of more practical relevance, similar mechanisms of field-particle interactions are expected. More importantly, the interactions are expected to become

stronger with the increasing ceramic loading of suspensions due to the decreasing inter-particle distance. A recent computational study for 20 vol.% aqueous Al_2O_3 suspensions showed similar particle self-assembly and chain formation due to DEP forces. [36] Currently, the authors are conducting a study on the AC electric field-assisted fabrication of freeze cast ceramics and the results will be communicated soon.

2.4 Conclusions

This study revealed assembly of Al_2O_3 particles in aqueous media subject to high frequency AC field for both coarse and fine particles. Formation of chains of particles due to inter-particle interactions occurred, and chain length increased with AC electric field strength and duration. Chains were aligned in the direction of field. A two-step process was involved in inter-particle interactions and assembly. First, nearby individual particles moved toward each other to form small chains oriented along the direction of the field. Next, small chains developed interconnections, resulting in the formation of longer chains. Chain formation was attributed to dielectrophoretic (DEP) forces. The current results revealed a marked effect of particle size on the "suspension microstructure", where decreasing inter-particle distance in fine particle suspension caused favorable conditions for assembly. Suspension microstructure was disrupted as soon as the field was removed, and higher field duration was associated with an improved pattern retention following the field removal. In a deliberately created spatially non-uniform AC field, coarse particles moved toward the regions of weaker field strength (negative-DEP), whereas fine particles migrated toward the regions of stronger field strength (positive-DEP). Thus, different mechanisms were responsible for chain formation for coarse and fine particles. The current research findings

provide invaluable insights into the interactions between AC electric field and ceramic particles in aqueous media for assembly.

CHAPTER 3

EFFECTS OF PARTICLE TYPE, FREQUENCY, AND DISPERSANT

3.1 Introduction

In the previous chapter only particle size, voltage and application time were investigated as variables for chain formation of alumina in AC field. However, the permittivity and conductivity of the particles and the suspension play a significant role in the formation of chains and dielectric forces. Assembly of colloidal particles is governed by the local interactions between particles and the underlying mechanism and strongly depends on both the specific properties of individual particles and their surrounding medium. [7,8] Application of an alternating current (AC) electric field to a media containing particles with electrical properties (permittivity and conductivity) is different than the media results in electric field non-uniformity. [14,15] To fully understand the mechanisms behind chain formation in ceramic particles it is necessary to investigate the effects of changing the properties of the media and particles. In this chapter chain formation of alumina is compared with barium titanate particles of the same size so that the effects of particle properties can be compared. [7,8] Alumina has relatively low permittivity and conductivity compared to barium titanate making them good particles for comparing these property differences. [27,28,29,30] Furthermore, frequency dependent effects were also not investigated in the previous chapter; however, from equations 1-5 in chapter 1 we can see that frequency has a role in the strength of the dielectric forces. Additionally, in chapter 2 using “MyDEP” software it can be seen

the CMF value changes with frequency. [21] It is possible that frequency could cause a crossover point at which a particle's motion shifts from n-DEP to p-DEP or vice-versa. [20,21]

Dilute suspensions were once again used to enable visualization of individual particles and their motion to study inter-particle interactions due to the application of AC field using an optical microscope. Particle motion was also further studied under a scanning electron microscope (SEM) by adding binder to the suspension and drying the chains while keeping them intact. This allowed them to be placed under SEM so that the individual small particles might be viewed to see how they made up the chains. AC field was applied through two identical coplanar, parallel metal electrodes, which created a spatially homogeneous electrical field perpendicular to the two metal electrodes in the absence of particles. However, a spatially non-uniform electric field was induced by the suspending particles. DEP behavior of the ceramic particles was investigated using dissimilar size electrodes for both particles, with and without dispersant at all frequencies. The current research findings provide insights into the interactions between high-frequency AC electric field and the properties of the medium and ceramic particles in aqueous media for particle motion and assembly at various frequencies.

3.2 Material Selection, Characterization, and Processing

Following the initial investigation into chain formation by DEP fields there remained quite a few variables left unexplored by those initial experiments. Namely the effects of the type of ceramic particle chosen, the frequency, and the addition of dispersant to the media. To begin with barium titanate $BaTiO_3$ was chosen as a second ceramic particle type for comparison against the alumina that had already been tested. The aqueous suspension concentration would remain very dilute (0.02 vol.%) since that was an effective suspension concentration for being able to visually

inspect the chains under the microscope. However, unlike the previous experiments, the ceramic suspensions would be mixed DI to make 0.5 vol. % suspensions first and then those more concentrated suspensions would be ball milled with Zirconium media for 24 hours prior to being diluted to make the 0.02 vol. % suspensions. This was important since dispersant would be added in some of the experiments and the processing methods would have to be kept consistent throughout all the trials. The fine Al_2O_3 powder (referred to as FA in the previous section, purchased from Inframat Advanced Materials, Amherst, NY) was once again selected for the first particle type. The second would be a similarly sized barium titanate particle from the same supplier. In both cases Inframat Advanced Materials is a reliable source for ceramic powders. Scanning electron microscope (SEM) images of alumina and barium titanate powders are shown in Fig. 3.1a and 1b, respectively. To confirm that both powders were approximately the same size, the size of the individual particles were measured from SEM images. The process for preparing the powder to be measured was described in Chapter 2 section 2 and the process for using Fiji - ImageJ® was described in Chapter 2 section 2 as well as in the supplemental materials it refers to. The powder size was then determined using the "particle analysis" plugin in Fiji - ImageJ®. For alumina powder, a total of 1800 particles were measured. Similarly, for barium titanate powder, a total of 2200 particles were measured. Based on these measurements, both particle size distribution and cumulative distribution of alumina and barium titanate powders are shown in Fig. 3.1e and 1f, respectively. For alumina particles, estimated d_{10}, d_{50} and d_{90} values were 0.15, 0.41 and 0.60 μm, respectively. For barium titanate particles, estimated d_{10}, d_{50} and d_{90} values were 0.11, 0.32 and 0.51 μm, respectively. Both particles were relatively similar in size and distribution making them easily comparable.

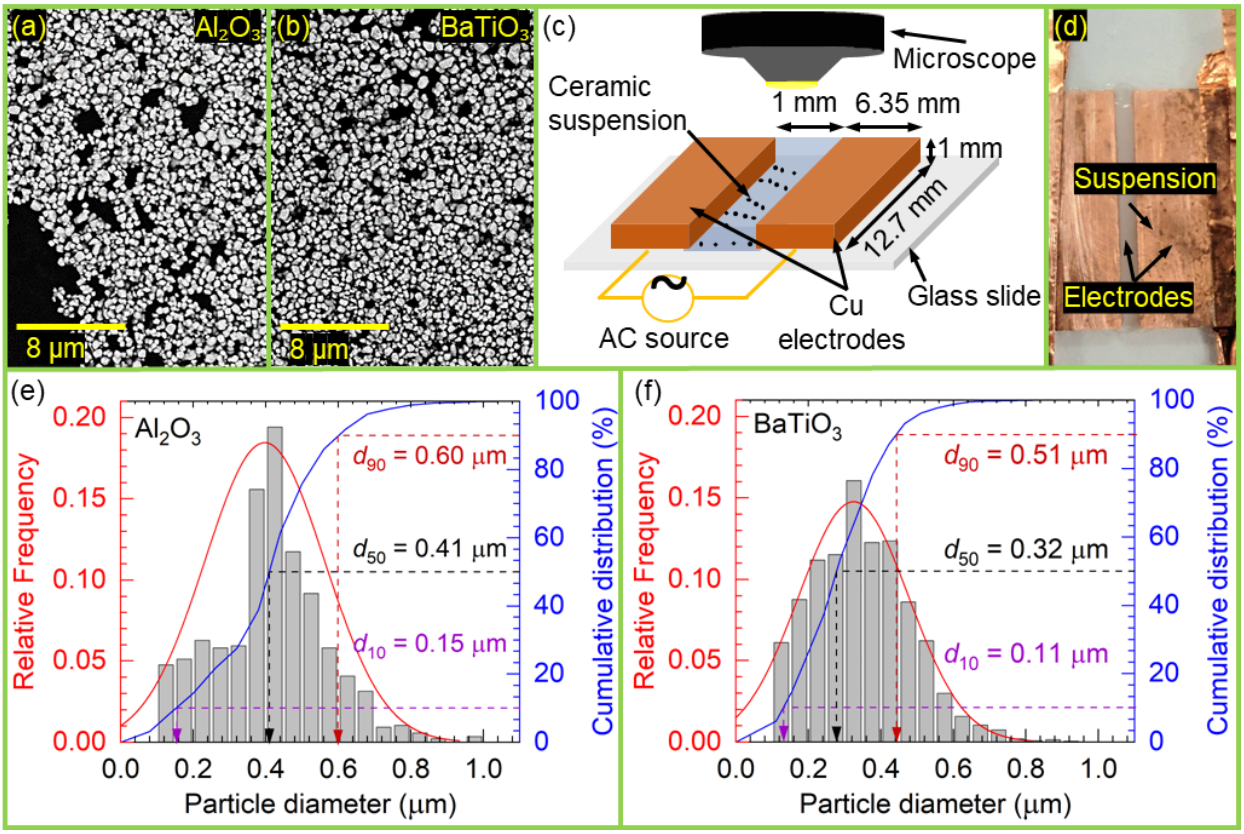

Fig. 3.1 Scanning electron microscope (SEM) image of (a) alumina powder and (b) barium titanate powder particles. (c) Schematic of experimental setup showing chains forming. (d) Optical image of the setup showing the copper electrodes, the suspension, and the optical microscope. Particle size distribution and cumulative distribution in (e and f) alumina powder and barium titanate powder

Like in chapter 2, Fig. 3.1c shows a schematic of the experimental setup, which consisted of two identical coplanar, parallel copper (Cu) electrodes attached to a glass slide. As described in Chapter 2 the Cu electrodes were once again of rectangular shape with 1 mm thickness and the gap between the electrodes was 1 mm. A function generator (Tektronix AFG 3102) and a voltage amplifier (Tegam model 2340) were used to apply an AC field, while voltages across the electrodes during the experiments were monitored through an oscilloscope (Tektronix TDS 1002). For each

experiment, the gap between Cu electrodes was filled with Al_2O_3 suspension and the suspension height was about 1 mm. Each experiment was *in situ* observed and recorded using an optical microscope (Leica DM6 M, Buffalo Grove, IL). An image of the Cu electrodes with Al_2O_3 suspension placed between the electrodes is shown in Fig. 3.1d.

To compare the effect of the different particle types on the formation of chains the applied peak-to-peak AC voltage (V_{pp}) was systematically changed to vary field strength (V/mm) and find the threshold value for each powder, where the threshold field strength was determined as the critical field strength where formation of particle–particle chains occurred through particle assembly. For both barium titanate and alumina suspensions, a series of studies were performed at various field strengths, frequencies, and with and without dispersant. However, the maximum field strength achieved (200 V/mm) was limited by the highest AC voltage that can be applied via the function generator and voltage amplifier used in this work. From the analyses of the videos of the experiments (recorded at 60 fps.) using the Leica optical microscope, the effects of particle size, field strength and field duration on inter-particle interactions and chain formation were quantified in terms of chain length and inter-chain distance. For each field strength and powder type, three experiments were performed to assess reproducibility.

Additionally, chains were preserved by adding an organic binder solution of 4 wt. % binder (poly-(2-ethyl-2-oxazoline) to the suspension. The addition of binder solution was determined to have a negligible effect on the formation of chains aside from making them more easily preserved. The preserving of chains was done by placing the electrode setup on a hotplate and then applying field. After 2 minutes had passed, the field was removed and the hotplate was used to evaporate off the water without boiling it. From there the dried chains could be placed in the scanning electron microscope (SEM). Scanning electron microscope images were taken of the chains (SEM,

Phenom Pure, Thermo Fisher Scientific) to more closely inspect the particle distribution before and after applying AC electric field. This was done to verify qualitatively the observations found under the optical microscope.

Additionally, the DEP behavior of alumina and barium titanate particles was investigated to determine whether the particles exhibited negative-DEP (n-DEP) or positive-DEP (p-DEP) behavior at a variety of frequencies with and without dispersant. To study DEP behavior, Cu electrodes of dissimilar size were used to deliberately apply spatially non-uniform AC field to aqueous Al_2O_3 suspensions and migration of particles in the suspensions and were observed using an optical microscope (Leica DM6 M, Buffalo Grove, IL). The table below shows the permittivity and conductivity for all particles and conditions where measurable or available in the literature.

	Electrical conductivity	Relative permittivity
DI water	$2.5x10^{-6}$ S/m	80.1 ε_0
Al_2O_3	$1x10^{-12}$ S/m	9.2 ε_0
$BaTiO_3$	1×10^{-7} S/m	6500 ε_0
Al2O3 Suspension	$2.5x10^{-6}$ S/m	-
$BaTiO_3$ Suspension	$2.5x10^{-6}$ S/m	-
Al_2O_3 Suspension with Dispersant	$15x10^{-6}$ S/m	-
$BaTiO_3$ Suspension with Dispersant	$15x10^{-6}$ S/m	-

Table 3.1 conductivity and permittivity properties [27,28,29,30]

From Table 3.1 we can see that while the addition of particles did not meaningfully change the conductivity of the suspension, the addition of even an extremely small amount of dispersant had a significant effect on the overall conductivity of the suspension. Furthermore, the conductivity and permittivity are significantly greater in barium titanate than in alumina. Based on this we can

predict that barium titanate should be more affected by dielectric forces compared to alumina based on the equations shown in chapter 1. [13,19,20,21,22]

3.3 Comparison of Particle Types on Chain Length

For alumina suspensions, optical images at three representative field strengths of 50 V/mm, 100 V/mm, 140 V/mm, and 200 V/mm are shown in Fig. 3.2 In this section, qualitative discussion is presented based on the observations from the optical microscope images, whereas quantitative analysis of chain length and inter-chain distance estimated from the images using ImageJ is presented in Fig. 3.5.

Compared to barium titanate particles, threshold field strength for alumina particles was lower, 24 V/mm compared to 50 V/mm, which is unexpected since the DEP force is proportional to the conductivity of the particles. However, this might be explained by the increased clumping in the solutions with the barium titanate particles, and this may have made it harder for them to form chains and for the particles to move freely. Barium titanate is more likely to clump in an aqueous suspension which may have had an impact on chain formation without dispersant being present to disperse the barium titanate particles and prevent clumping. At comparable field strengths, it appears that barium titanate chains had a greater separation from one another. At higher field strengths, these gaps become more pronounced, and it appeared that barium titanate chains were much more distinct which may have made it more difficult for the remaining chains to come together. Fig. 3.3.

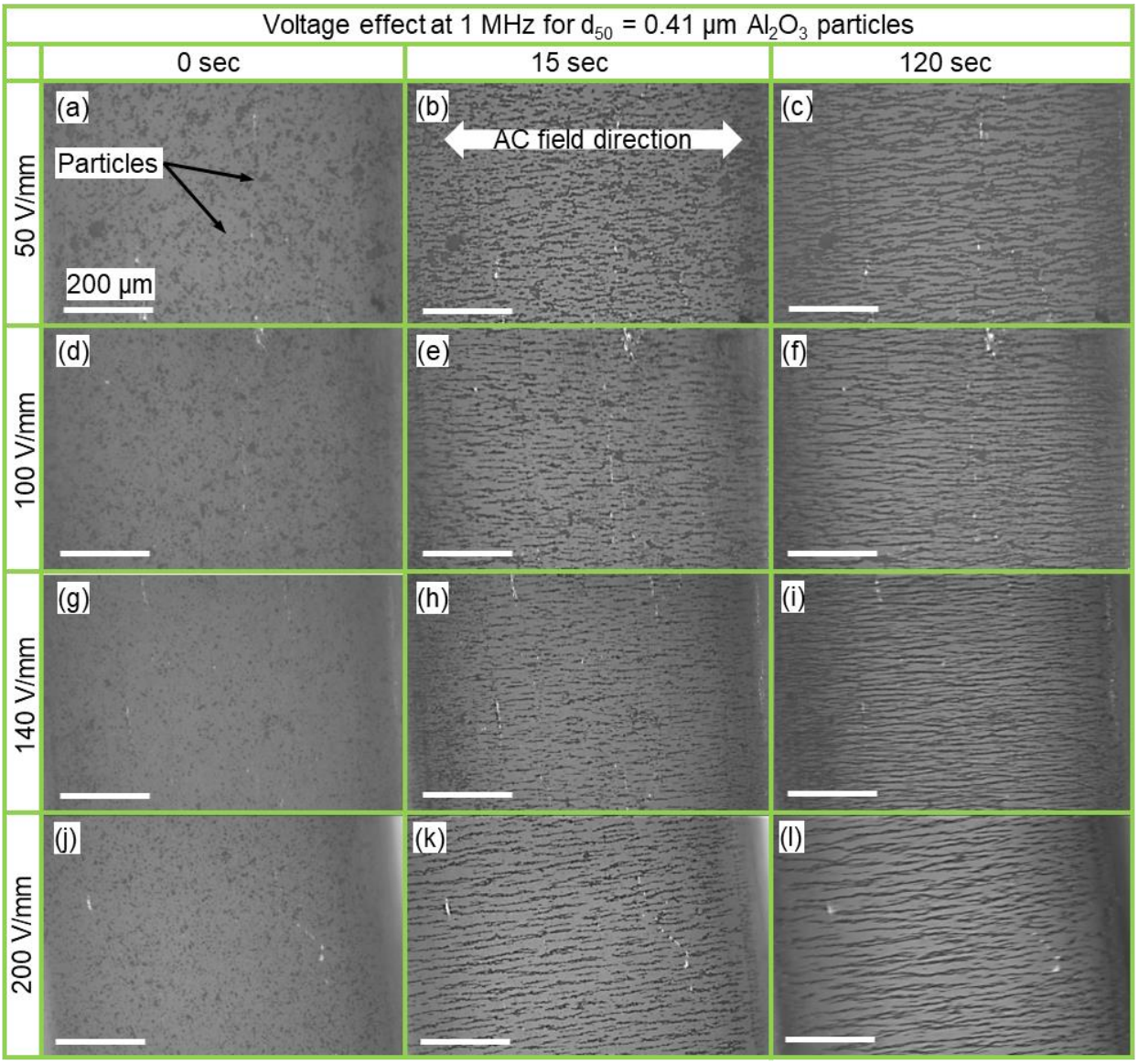

Fig. 3.2 Optical microscope images showing inter-particle interaction in alumina suspensions subject to 1 MHz AC field at representative field strengths of 50 V/mm (a–c), 100 V/mm (d–f), 140 V/mm (g–i), and 200 V/mm (j–l). In (a–i), images in the left column show distribution of particles prior to field application.

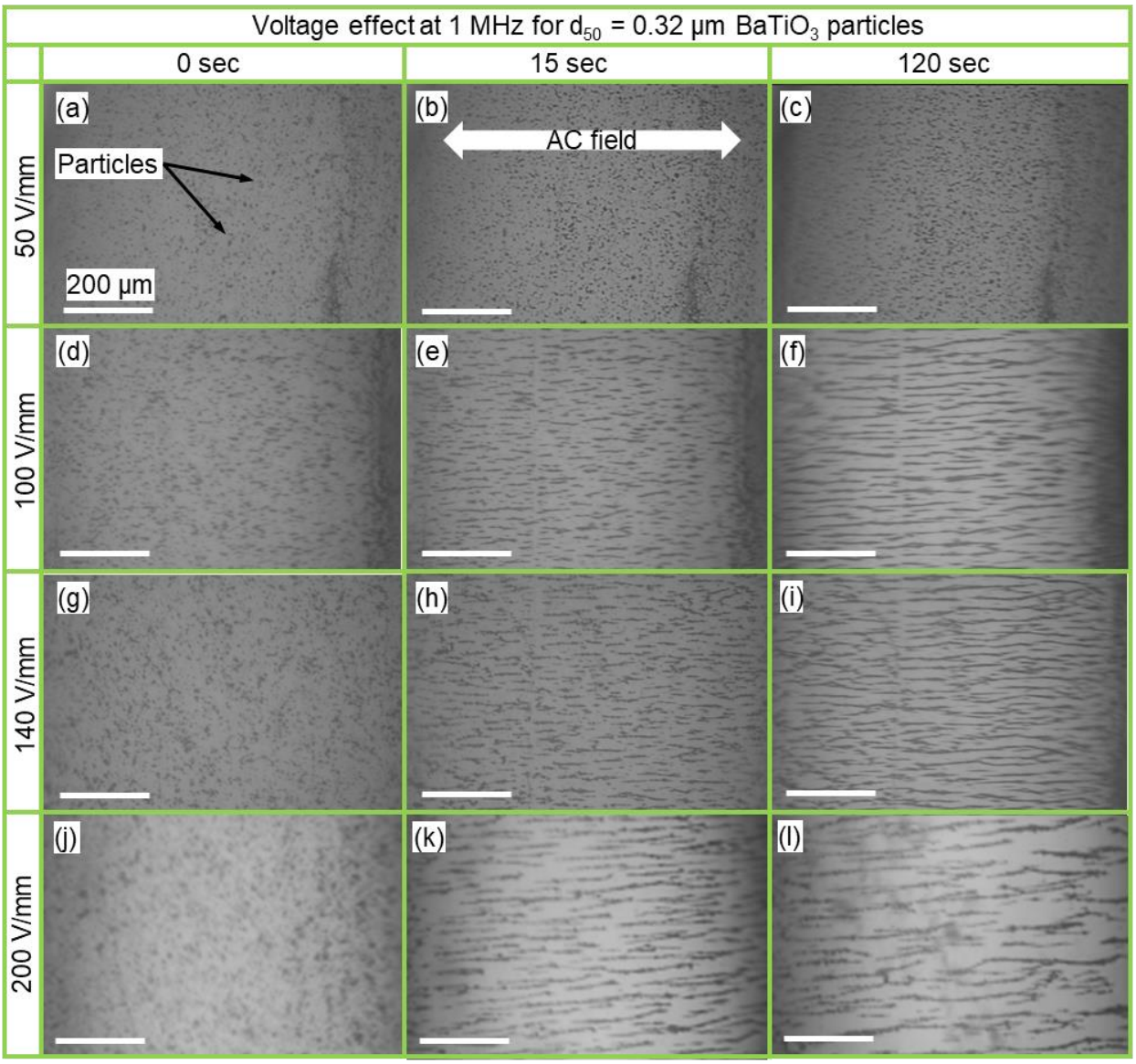

Fig. 3.3 Optical microscope images showing inter-particle interaction in barium titanate suspensions subject to 1 MHz AC field at representative field strengths of 50 V/mm (a–c), 100 V/mm (d–f), 140 V/mm (g–i), and 200 V/mm (j–l). In (a–i), images in the left column show distribution of particles prior to field application.

The small size of the alumina and barium titanate particles as well as the fine microstructure of the chains prompted the use of SEM images to look at the finer details of the chain microstructures, Fig. 3.4. To preserve the chain structures after evaporating the water from the

electrode setups a small amount of binder (2 vol. %) was introduced into the suspension. While this small amount of binder may have had some effect on the particles forming chains it was visually observed to be small enough that the images obtained could be reasonable representations of the chains formed without binder.

In Fig. 3.4 SEM images were taken of the powder before and after application of an electric field and at two magnifications showing the chains. Based on the optical microscope images it was predicted that barium titanate chains would be thicker and contain more particles compared to the alumina chains. It was predicted that this might be the case based on the higher dielectric properties of the barium titanate particles when compared to the alumina particles. In Fig. 3.4a-b and d-e the loose agglomerations of particles for both barium titanate and alumina were able to form chains that were able to be preserved for viewing under SEM. The SEM images in Fig. 3.4 below visually confirmed that compared to alumina chains (Fig. 3.4c) the barium titanate chains (Fig. 3.4f) were much thicker and were made up of more individual particles compared to the alumina chains. This suggests that the barium titanate particles were more attracted to each other and that individual chains of barium titanate particles moved together to form thicker chains with one another over time in the AC electric field.

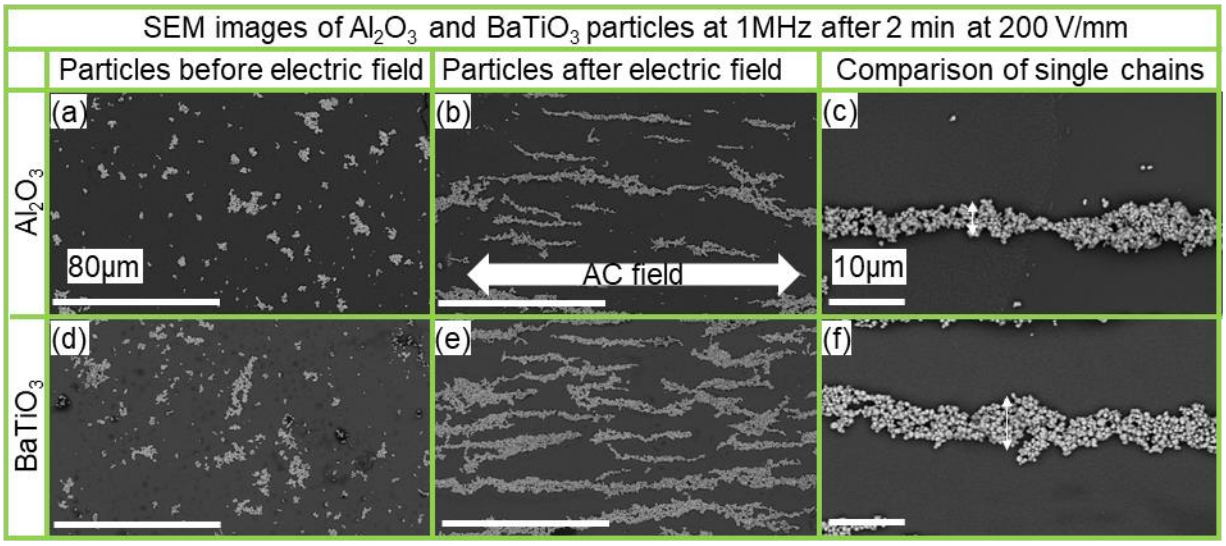

Fig. 3.4 SEM images revealing inter-particle interaction in alumina suspensions subject to 1 MHz AC field at 200 V/mm. In (a and d), SEM images in the left column show distribution of particles prior to field application. In b and e chains are shown at 1000x magnification and at 5000x magnification in c and f.

The current results revealed a difference in the "suspension microstructure" between barium titanate and alumina suspensions with significantly thicker chains forming at larger inter-chain distances between barium titanate chains. Differences between suspension microstructures were quantified from image analysis in terms of chain length and inter-chain distance.

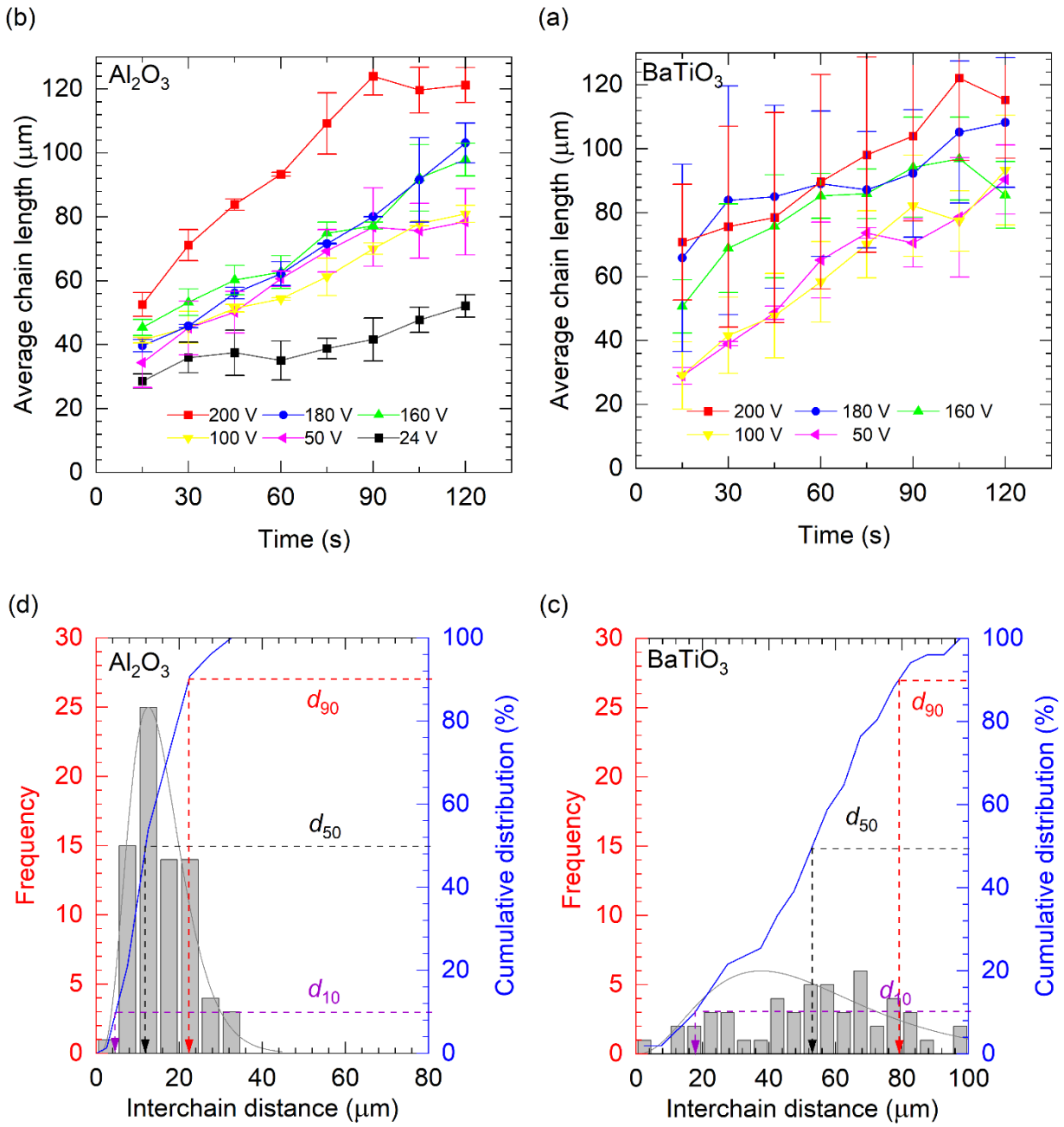

Fig. 3.5 Variation in chain length with field duration in (a) alumina and (b) barium titanate suspensions at various field strengths. The distribution and cumulative distribution of inter-chain distances perpendicular to the field direction after 120 s at 200 V/mm for (c) alumina and (d) barium titanate suspensions

Fig. 3.5a and b shows average chain length evolution with field duration in alumina and barium titanate suspensions, respectively, at various field strengths. Standard deviation in chain length was greater in barium titanate than in alumina at 200 V/mm, the maximum chain length was observed to be about 120 μm when the field duration was 120 seconds for both particle types. At all observed field strengths, the barium titanate particles and alumina particles had comparable values for chain length. This was an unexpected outcome since the barium titanate particles had greater dielectric properties. However, the chain in properties had a much greater effect on inter-chain distance than on chain length.

Fig. 3.5c and d show distribution of inter-chain distances (measured perpendicular to field direction between two adjacent chains) and cumulative distribution in alumina and barium titanate suspensions, respectively, at two minutes for the field strength of 200 V/mm. Inter-chain distance distribution was relatively symmetric in alumina suggesting a relatively homogeneous suspension microstructure in the suspension. Comparatively, barium titanate had an extremely wide range of inter-chain distances indicating a more uneven random spread of inter-chain distances. The increased inter-chain distances were qualitatively assessed as being caused by thicker chains having attracted more chains and thus more particles around them to come together. This is also likely the reason that barium titanate chains had a much greater range in lengths and larger standard deviation compared to alumina since the structure was less even and regular. This is likely the result of barium titanate having greater dielectric properties compared to alumina. As shown in Fig. 2.2 the particles first form small chains and then those chains group together to form larger chains. Since barium titanate has greater dielectric properties the barium titanate chains should be expected to have greater inter-chain forces. As these inter-chain forces pull nearby chains together to form thicker and, in some cases, longer chains we can expect to see barium titanate chains group

together leaving more space between them until the inter-chain forces are no longer great enough to pull progressively farther chains together. This would explain why barium titanate has such large inter-chain distances since the closer chains would have combined with one another. This does not, however, explain the wide range in inter-chain distances. The wide range of inter-chain distances can be explained by the initial clumping visible in the barium titanate suspension. The clumping makes the distribution of particles less even which leads to a less even distribution of chains. This also might make some chains more stationary since it takes much greater dielectric and inter-particle forces to move the agglomerate particles clumps. The quantitative image analysis reinforces this assessment that at the same field strength, barium titanate chains had a greater attraction to one another, and more particles came together to form each chain, attesting to the influence of particle type on the AC field-induced ceramic suspension microstructure.

3.4 Frequency Effect on Chain Formation and Particle Motion

From equations 1- 5 in the introduction it can be shown that the dielectric forces on the particles that lead to chain formation are related to the frequency of the applied field. From equations 3 and 4 it is shown that increasing frequency leads to a decrease in the complex permittivity of the particles. This suggests that as frequency increases the Clausius-Mossotti factor would decrease which may lead to a change in the field effects on the particles depending on whether they are experiencing p-DEP or n-DEP.

In Fig. 3.6 the chain formation of alumina particles is shown at 200 V/mm four different frequencies 250 kHz a-c, 500 kHz d-f, 750 kHz g-i, and 1 MHz j-l. The 1 MHz frequency has served as the baseline condition for all the experiments thus far and was the highest frequency

achievable at 200 V/mm. In Fig. 3.6 a-c for at 250 kHz it was observed that there was a significant amount of fluid motion present during the experiment.

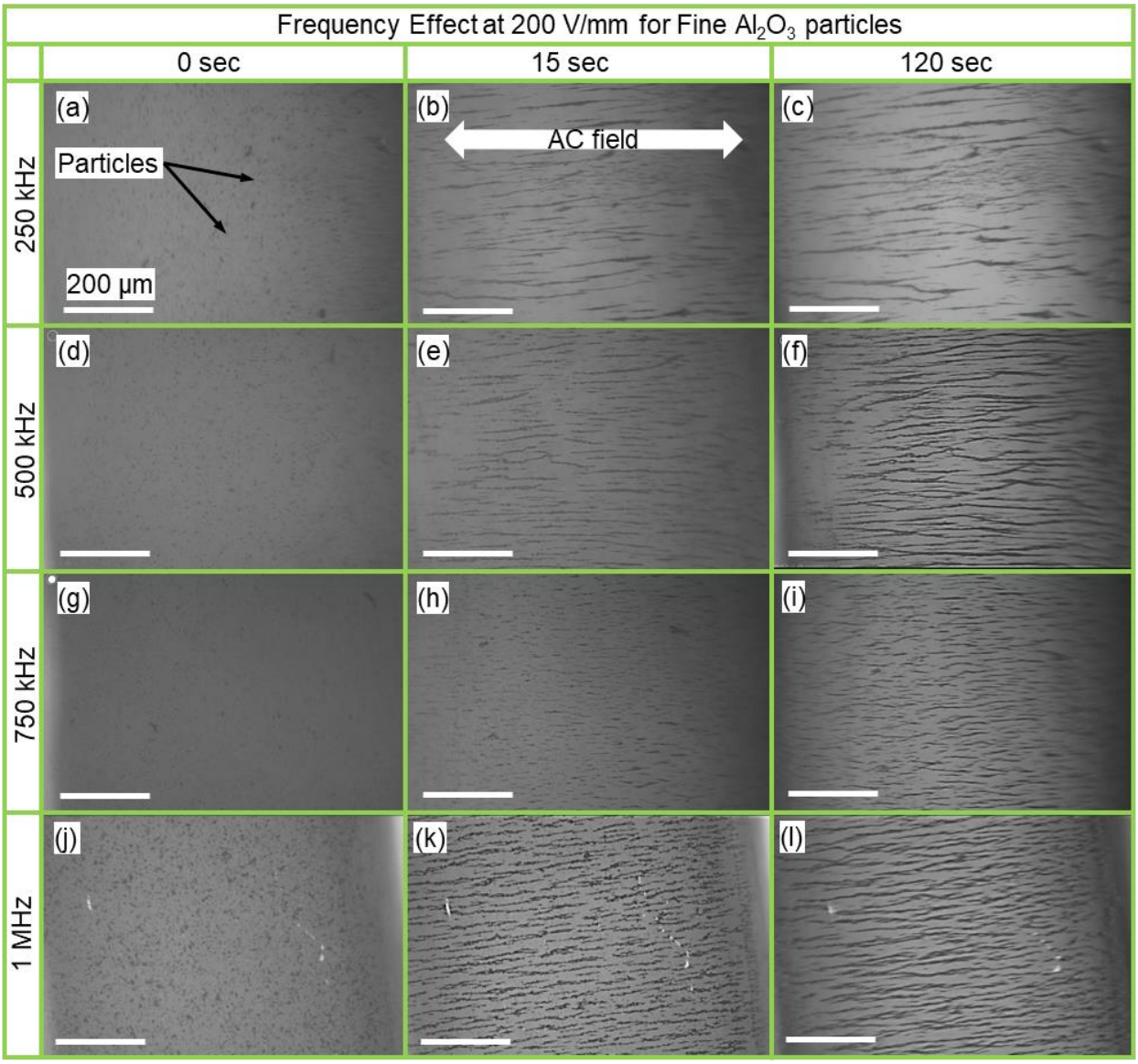

Fig. 3.6 Optical microscope images revealing inter-particle interaction in alumina suspensions subject to 200 V/mm AC field at representative frequencies of 250 kHz (a–c), 500 kHz (d–f), 750 kHz (g–i), and 1 MHz (j-l). In (a–i), images in the left column show distribution of particles prior to field application.

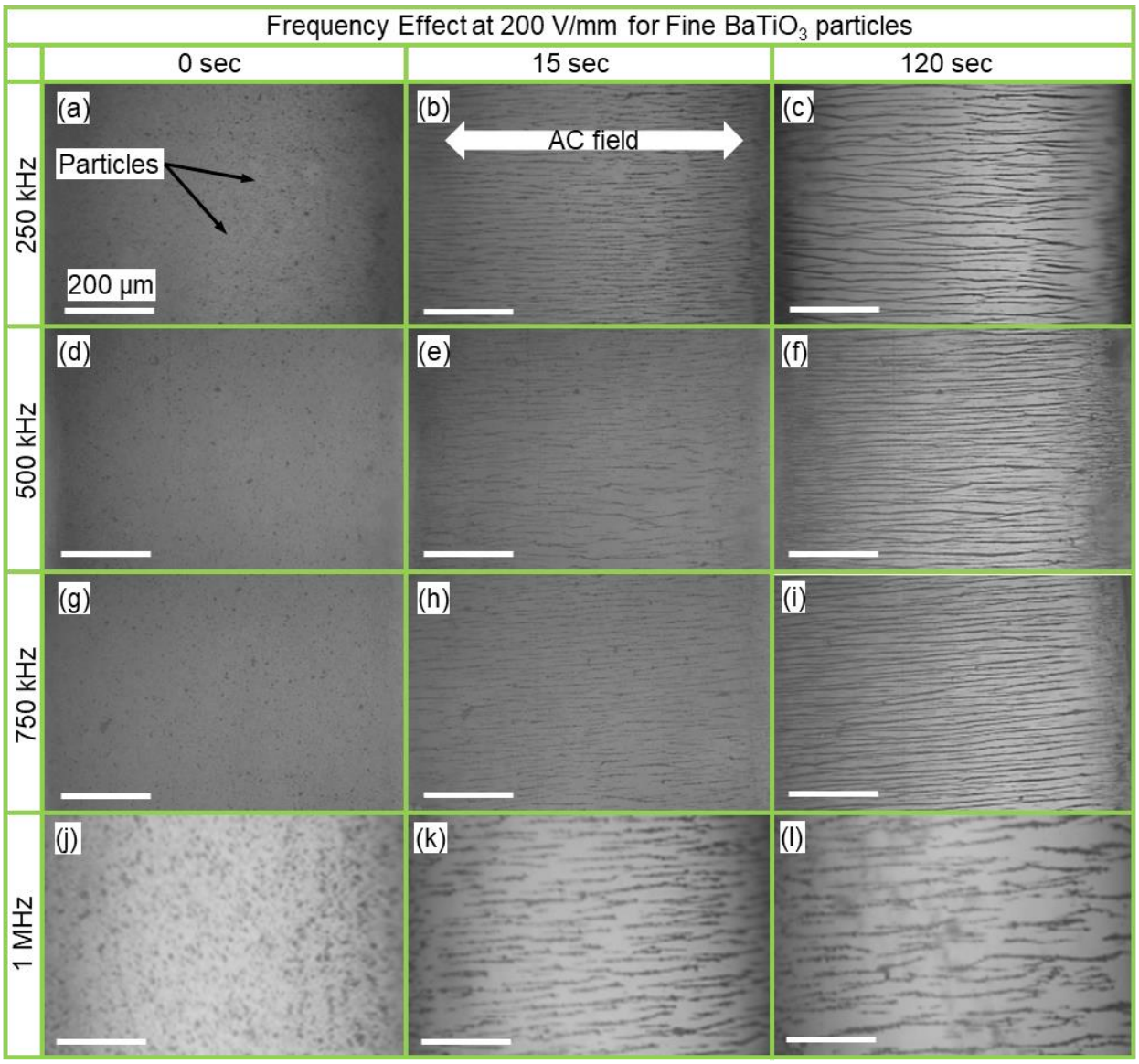

Fig. 3.7 Optical microscope images revealing inter-particle interaction in barium titanate suspensions subject to 200 V/mm AC field at representative frequencies of 250 kHz (A–C), 500 kHz (D–F), 750 kHz (G–I), and 1 MHz (j-L). In (A–I), images in the left column show distribution of particles prior to field application.

As seen in Fig. 3.6, the fluid motion greatly impeded chains from forming and disrupted chains that did form over the course of the 2-minute duration. This increase in fluid motion likely has

two major causes. Primarily, the decrease in frequency caused slower transitions between the direction of the field. This change in motion back and forth between the electrodes resulted in a wave-like fluid motion where fluid moved back and forth between the electrodes. Furthermore, electrolysis at the electrode surfaces is more extreme at lower frequencies likely leading to a greater magnitude of fluid motion.

The effects of the fluid motion are shown to decrease with increasing frequency as shown in Fig. 3.6c, f, i, and l. In Fig. 3.6 g-l between 750 kHz and 1 MHz there is relatively little difference in fluid motion and therefore relatively little difference visible in the suspension microstructure. In Fig. 3.7 the chain formation of barium titanate particles is shown at 200 V/mm four different frequencies 250 kHz a-c, 500 kHz d-f, 750 kHz g-i, and 1 MHz j-l. As mentioned previously, 1 MHz frequency has served as the baseline condition for all the experiments thus far with barium titanate In Fig. 3.7a-c for at 250 kHz and it was once again observed that there was a significant amount of fluid motion present during the experiment like with the alumina. This fluid motion greatly impeded chains from forming and disrupted chains that did form over the course of the 2-minute duration, but visually it was observed that the increase in fluid motion did distribute barium titanate particles more evenly and produce a finer microstructure. This means that there is potential for using frequency with barium titanate to tailor the suspension microstructure.

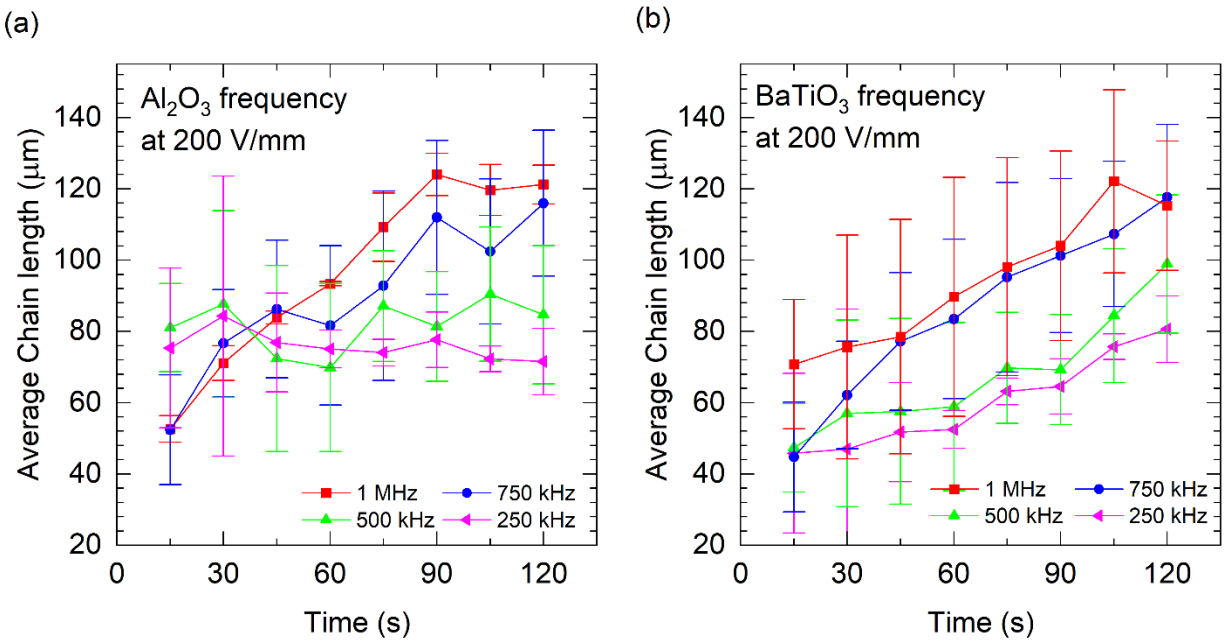

Fig. 3.8 Variation in chain length with field duration comparing alumina (a) and barium titanate (b) suspensions and the relative change due to frequency between 1 MHz and 250 kHz at a constant field strength of 200 V/mm.

Overall, frequency appears to visually make a significant difference in the suspension microstructure and chain formation of both barium titanate and alumina particles. These observations were quantified in Fig. 3.8a and b which show average chain length evolution with field duration in alumina and barium titanate suspensions, respectively, at various frequencies. For both barium titanate and alumina, chain length significantly decreased with the decrease in frequency. In both cases chain lengths for barium titanate and alumina at 1 MHz were about 120 µm whereas at 250 kHz chain lengths dropped to 70 – 80 µm. However, the decrease in chain length with frequency can be seen to be almost nonexistent between 1 MHz and 750 kHz showing that there is a range in frequency for which there is very little effect on the chain formation. This indicates that there may be a diminishing effect of increasing frequency as the fluid motion decreases to a point where it no longer impacts the formation of chains. The quantitative image

analysis reinforces that chain formation for all particles tested is negatively affected by decreasing the frequency, attesting to the influence of frequency on AC field induced ceramic suspension microstructure.

3.5 Dispersant Effect on Chain Length

As mentioned in the introduction, colloidal processing usually involves the addition of dispersants to the suspension to stabilize it. These dispersants affect the surface potential and conductivity of the suspensions. The surface potential and suspension conductivity also play a role in DEP forces, so it is important to evaluate the effect that adding dispersants to the suspension will have on chain formation and particle motion. Furthermore, the addition of an electrolyte such as a salt, an acid or a base can cause electrolysis to increase in AC electric fields. Therefore, it was important to observe if the addition of dispersant would cause electrolysis that might impact the formation of chains.

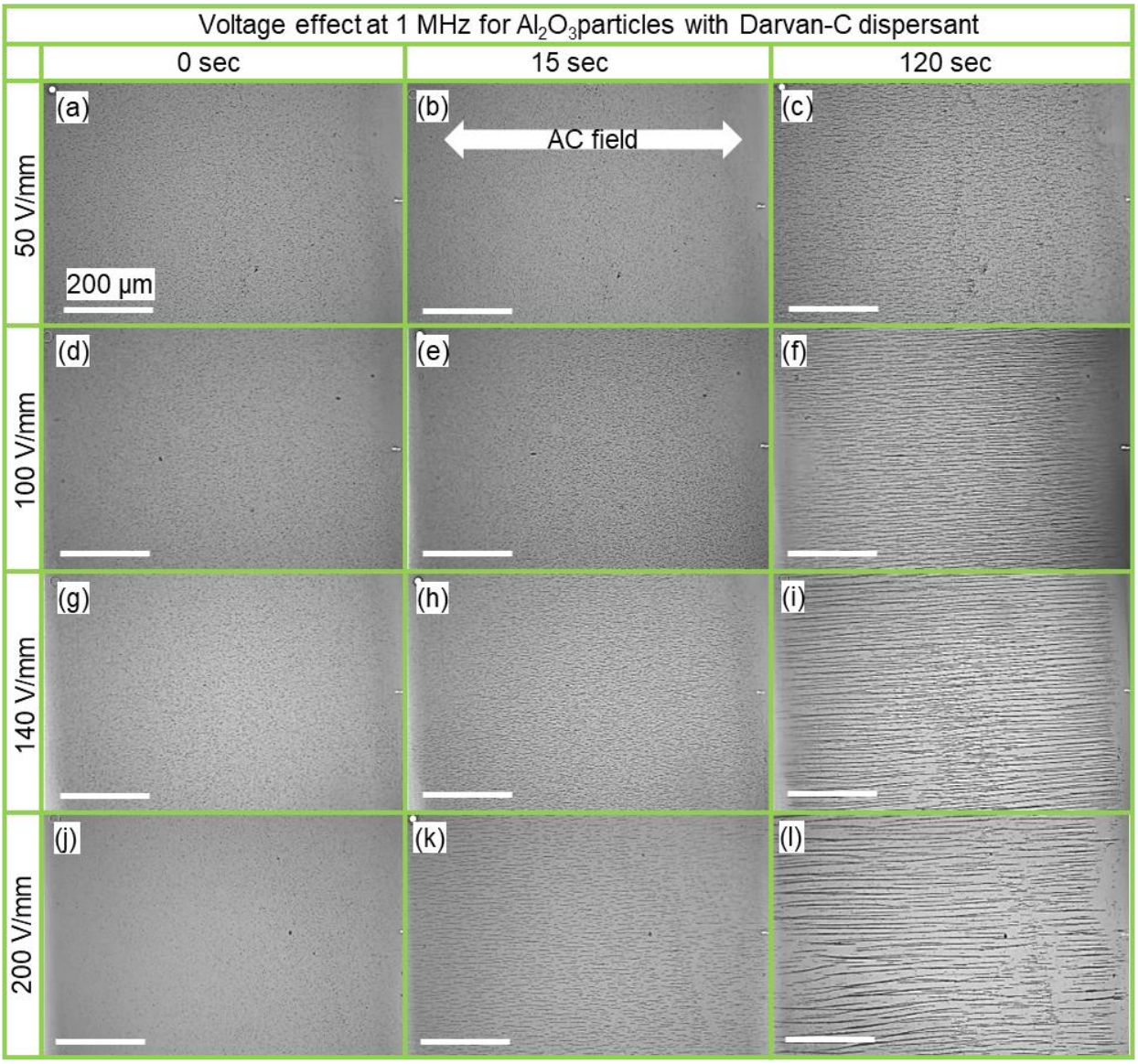

Fig. 3.9 Optical microscope images showing inter-particle interaction in alumina suspensions with dispersant subject to 1 MHz AC field at representative field strengths of 50 V/mm (a–c), 100 V/mm (d–f), 140 V/mm (g–i), and 200 V/mm (j–l). In (a–i), images in the left column show distribution of particles prior to field application.

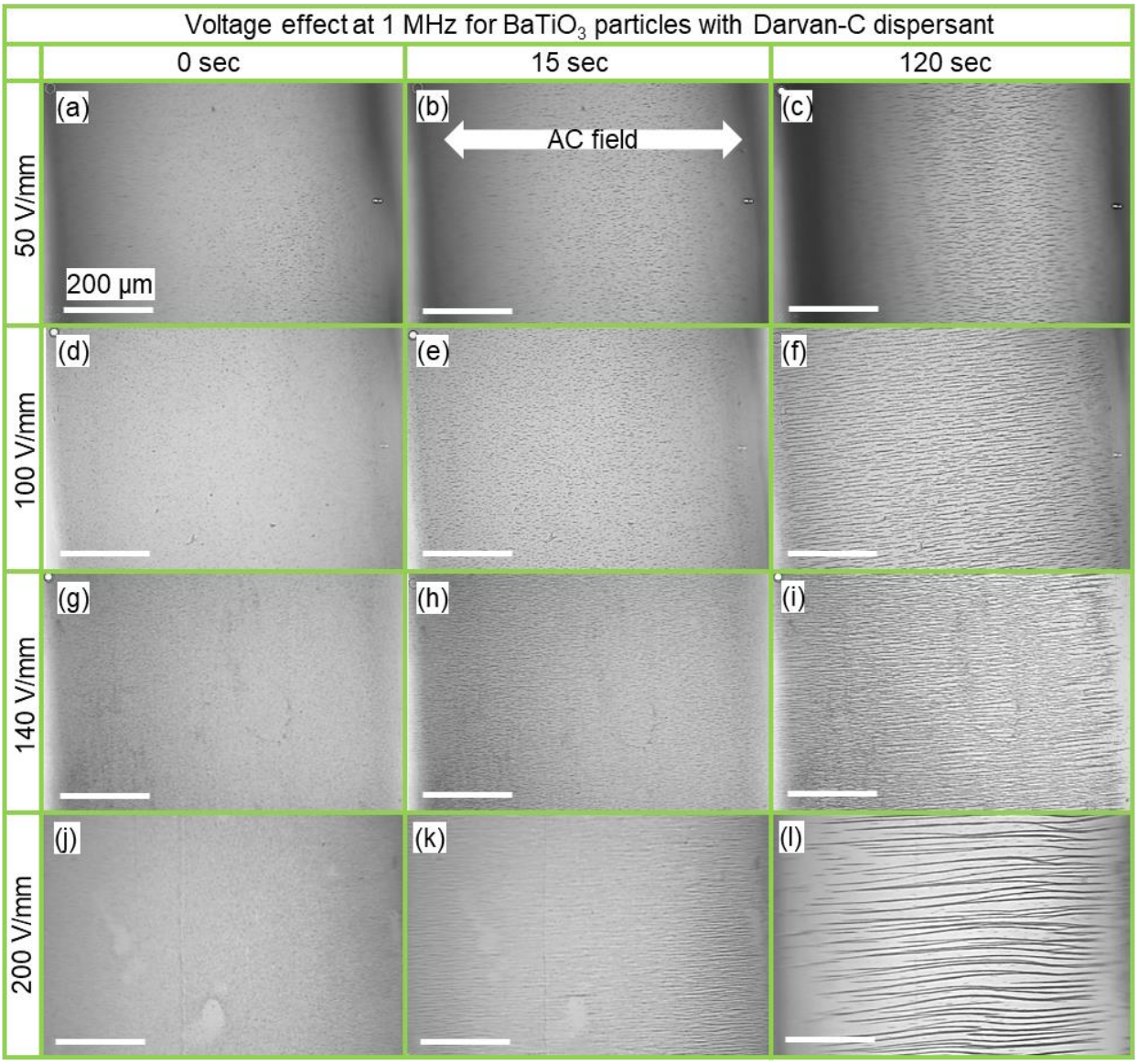

Fig. 3.10 Optical microscope images revealing inter-particle interaction in barium titanate suspensions with dispersant subject to 1 MHz AC field at representative field strengths of 50 V/mm (a–c), 100 V/mm (d–f), 140 V/mm (g–i), and 200 V/mm (j–l). In (a–i), images in the left column show distribution of particles prior to field application.

From the optical microscope images, we saw that at all field strengths tested from 50 to 200 V/mm chains formed, and significant effects from electrolysis were not visible. In Fig. 3.10a,

d, g, j it is clearly shown that dispersant caused a significant difference in the initial suspension microstructure. The addition of the dispersant made the suspension more stable and thus only a few small agglomerates formed compared to the suspensions without dispersant. Furthermore, this lack of agglomerates significantly affected the formation of chains and the final suspension microstructure within the chains. It was observed that particles were able to move much more freely in the suspension and formed much larger chains compared to not using the dispersant. A finer suspension microstructure also formed as a result of adding dispersant, and chains were more distinctive and less clumped and interconnected than without the dispersant.

The addition of dispersant to barium titanate caused similar changes to what was previously observed in alumina. Like with alumina the particles were much more evenly distributed and the suspension microstructure contained fewer agglomerates or clumps. The chains were also longer and finer with relatively smaller inter-chain distances compared to barium titanate without dispersant, but they were still larger than the inter-chain distances between alumina. Unlike alumina at the higher voltage conditions a wave-like pattern formed which may have been a result of the interactions between the higher conductivity suspension and the more electrically active particles.

Quantitative measurements of chain length in Fig. 3.11a and b showed that alumina chains reached average lengths of ~180 μm at 200 V/mm at 2 min. and ~220 μm at 200 V/mm at 2 min. for barium titanate. Additionally, both barium titanate and alumina had almost 2 times larger chain lengths at 200 V/mm compared to without dispersant. Interestingly, chain lengths were much lower below 180 V/mm and were comparable to chain lengths without dispersant. This may be because the particles are able to move more freely in the suspension, so more voltage is required to hold the chains together.

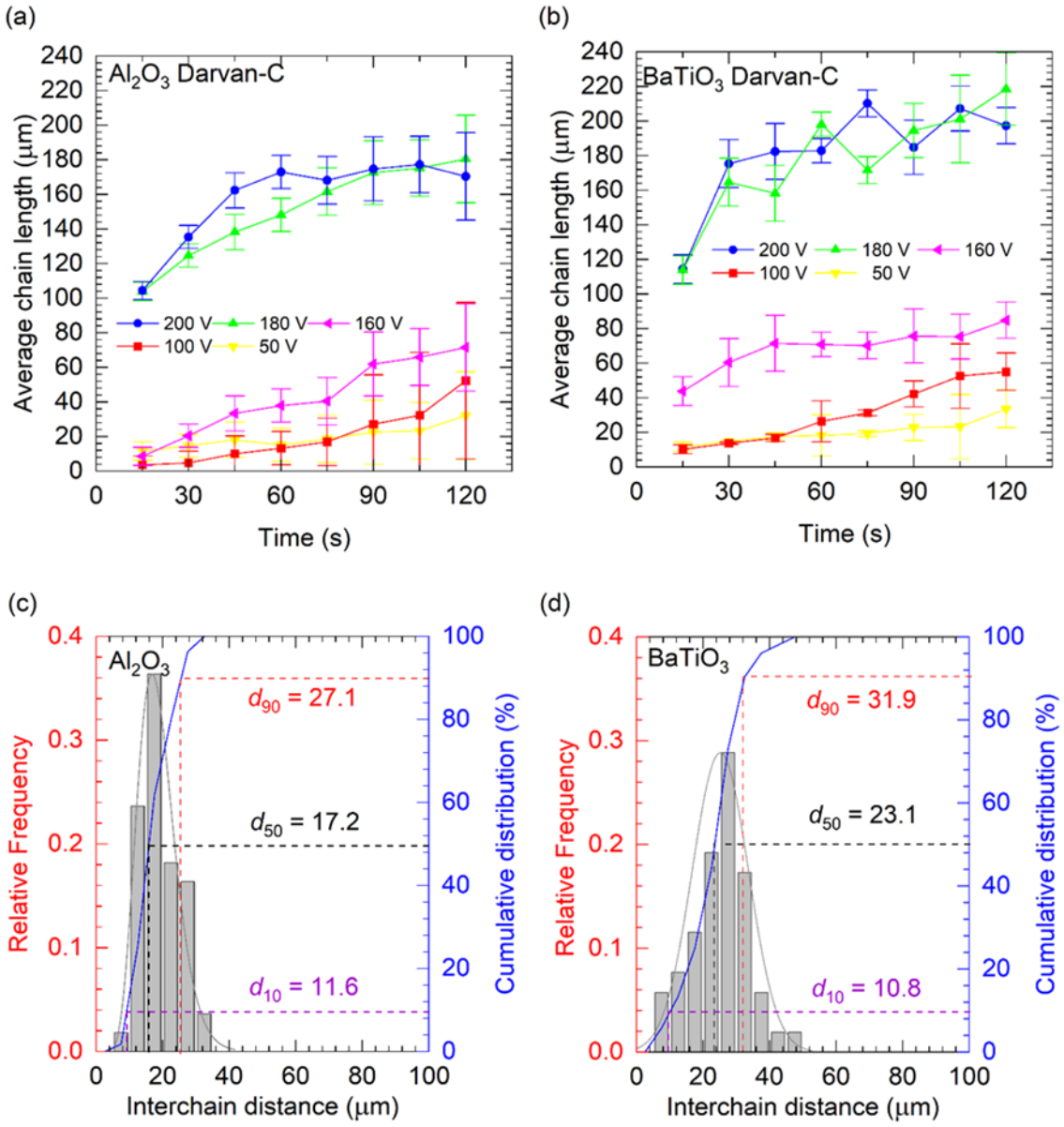

Fig. 3.11 Variation in chain length with field duration in (a) alumina and (b) barium titanate suspensions with dispersant at various field strengths. The distribution and cumulative distribution of inter-chain distances perpendicular to the field direction after 120 s at 200 V/mm for (c) alumina and (d) barium titanate suspensions

Fig. 3.11 c and d show distribution of inter-chain distances (measured perpendicular to field direction between two adjacent chains) and cumulative distribution in alumina and barium titanate

suspensions with dispersant, respectively, at 120 seconds for the field strength of 200 V/mm. For alumina suspension the d_{10}, d_{50} and d_{90} values for inter-chain distances were found to be 11.6, 17.2 and 27.1 μm, respectively. For barium titanate suspension, d_{10}, d_{50} and d_{90} values for inter-chain distances were 10.8, 23.1 and 31.9 μm, respectively. Unlike in barium titanate suspensions without dispersant, inter-chain distance distribution was relatively symmetric in both suspensions, suggesting a relatively homogeneous suspension microstructure in the former suspension. However, while barium titanate inter-chain distances significantly decreased in both range and size distances for alumina the addition of dispersant increased inter-chain distances and decreased the range of size. Furthermore, the difference in inter-chain distance between barium titanate and alumina was relatively small. This suggests that the effect of dispersant concentration was a more dominant effect compared to particle type. Quantitative image analysis showed that dispersant had an extremely significant effect on the AC field-induced ceramic suspension microstructure and suggested that this effect may be somewhat uniform across particle types with only a few differences. This increase in the similarity of the particles may be a result of them having relatively more similar dielectric properties after the addition of dispersant. Since ceramics have relatively low conductivity in general, with the addition of dispersant this conductivity is greatly increased with respect to the surface conductivity of the particles. [19,21,22,31] In particle processing this increase in surface conductivity is used to make suspensions more stable. It was observed that in left columns of Fig. 3.9 and 3.10 that the barium titanate and alumina particles were distributed similarly evenly indicating that they likely experience a comparable effect from the dispersant with respect to their change in surface conductivities. [27, 28, 29, 30, 32] All these factors likely result in the more relatively homogenous properties between the two particle types with the addition of dispersant. The differences in chain size that remain between alumina and barium titanate can be

seen at the higher voltage. Barium titanate can be seen to exhibit thicker slightly curved chains relative to alumina. Despite the addition of dispersant, barium titanate still has a much greater permittivity compared to alumina which may be the cause for these differences.

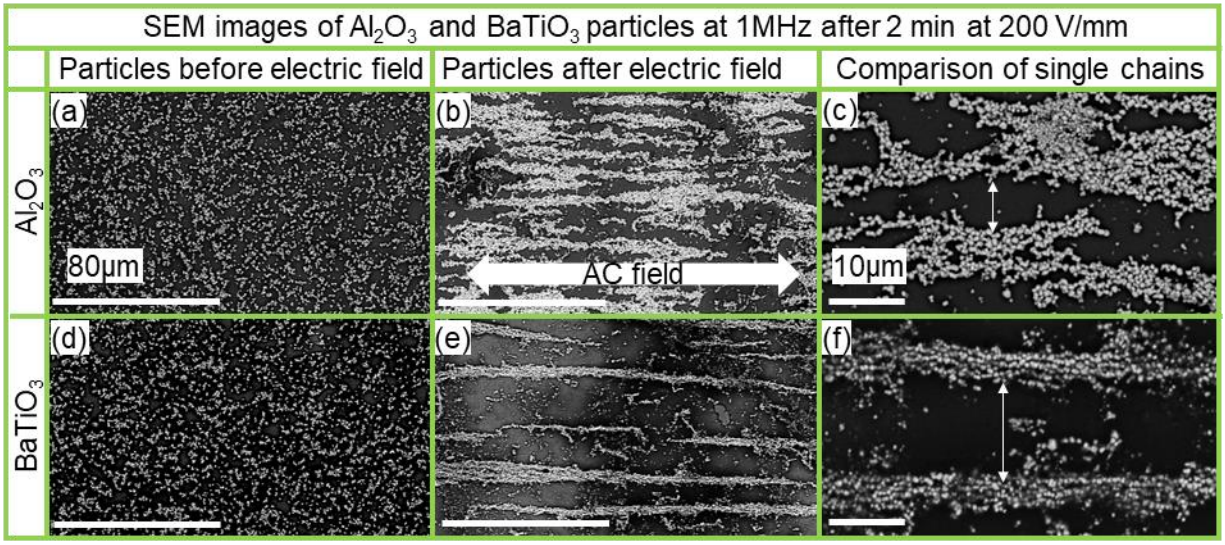

Fig. 3.12 SEM images revealing inter-particle interaction in alumina suspensions subject to 1 MHz AC field at 200 V/mm. In (a and d), SEM images in the left column show distribution of particles prior to field application. In b and e chains are shown at 1000x magnification and at 5000x magnification in c and f.

In Fig. 3.12 SEM images were taken of the powder before and after application of electric field with dispersant and at two magnifications showing the chains like in Fig. 3.4. Preserving the chains was more difficult for these suspensions since the dispersant made the particles more mobile in the suspension. In the optical microscope images, it was observed that barium titanate chains were farther apart and had a wave-like curve compared to the alumina chains. It was proposed that this might be the case based on the higher dielectric properties of the barium titanate particles when compared to the alumina particles interacting with the higher conductivity of the suspension after

adding dispersant. However, the wave-like structures were difficult to preserve for SEM due to those fine details being fragile. Some wave-like curvature can still be seen though, verifying that this curvature was present in the suspension microstructure. In Fig. 3.12a and d the particles for both barium titanate and alumina were shown to be far more evenly distributed compared to not using dispersant. Comparing the SEM images taken in Fig. 3.12 b-c and e-f it can be visually confirmed that compared to the alumina chains, the barium titanate chains were spaced farther apart confirming what was seen in optical images.

3.6 DEP Classification and Particle Motion in Non-uniform Fields

In the previous experiments in this section, AC field was applied via two identical coplanar, parallel electrodes, and chain formation occurred for all conditions. However, to identify n-DEP and p-DEP, a non-uniform AC field is required to study the mechanisms behind the particle motion. Although n-DEP and p-DEP interactions have resulted in assembly and chain formation, changes in experimental conditions could result in different mechanisms for chain formation.

The propensity for particles to exhibit n-DEP or p-DEP behavior depends on the sign of CMF, where CMF is positive and negative for p-DEP and n-DEP, respectively. From equations (2 – 4), magnitude and sign of CMF depends on the electrical properties (permittivity and conductivity) of the particles and the media as well as the frequency of the applied field. The frequency at which the CMF shifts between a positive value and a negative value is called the crossover frequency. In Chapter 2, it was shown that calculated values for CMF based on bulk values may not accurately represent the particles' behavior. However, from looking at the properties of particles and media we might be able to infer some things about particle motion.

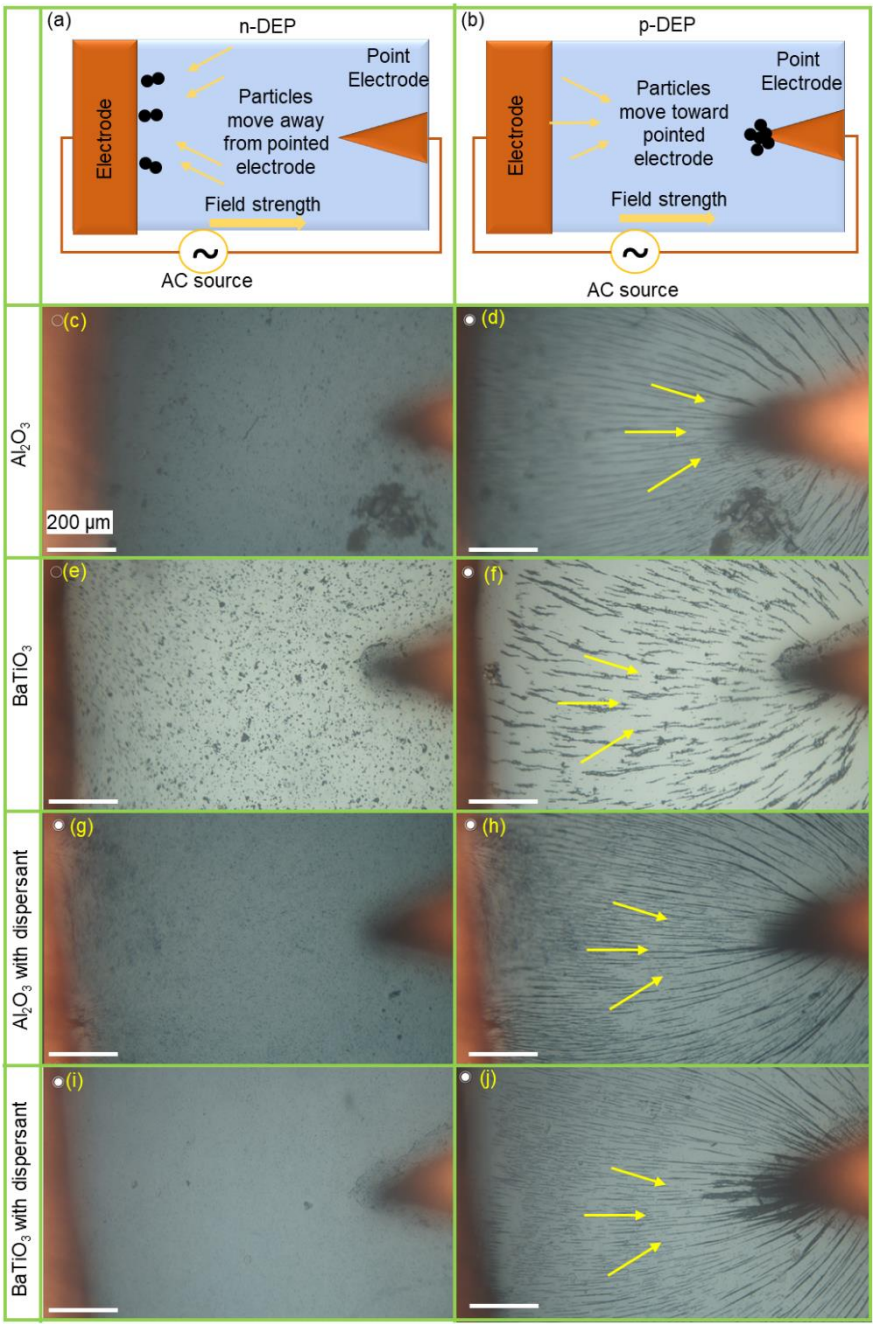

Fig. 3.13 Illustrative schematic of particle motion for (a) n-DEP and (b) p-DEP behavior of particles in non-uniform AC field. Application of field on (c–d) alumina and (e–f) barium titanate suspensions over 60 s. As well as alumina and barium titanate suspensions with dispersant added (g-h) and (i-j), respectively.

Electrical conductivity and relative permittivity of bulk Al_2O_3 were taken as $1x10^{-12}$ S/m and 9.2, respectively.[23, 24] Relative permittivity of DI water was taken as 80.1, whereas electrical conductivity of DI water was experimentally determined to be $2.5x10^{-6}$ S/m measured using a conductivity meter (HI2255, HANNA Instruments, Smithfield, RI). After adding dispersant, the conductivity increased to $10x10^{-6}$ S/m which is a 4x increase in conductivity.

Fig. 3.13a and b schematically illustrate n-DEP and p-DEP behavior of particles respectively. The setup consisted of a triangular pointed electrode (right) and a rectangular plate electrode (left) attached to a glass slide. The electrodes were coplanar, and the gap between the sharp end of the triangular electrode and the plate electrode was approximately 1 mm. The AC field with this electrode configuration is strongest near the sharp end of the triangular electrode and weakest near the plate electrode. For n-DEP behavior, particles would move toward the plate electrode, i.e., toward the regions of weaker field strength (Fig. 3.13a.) and for p-DEP behavior, the particles would move toward the region of stronger field strength near the point electrode, Fig. 3.13b. Fig. 3.13c and d show the distribution of alumina particles before and after field application for 60 seconds at 1 MHz, respectively. Similarly, Fig. 3.13e and f show the distribution of barium titanate particles before and after field application for 60 seconds at 1 MHz, respectively. In both cases the particles migrated to the pointed electrode (Fig. 3.13b), which suggested p-DEP behavior at 1 MHz. This makes sense when we consider that both particles are the same size and that size is a significant factor both from observations on size effects in Chapter 2 as well as from the equations in the introduction. Additionally, it makes sense that barium titanate would be likely to have p-DEP since its dielectric properties are greater than those of alumina. These tests were then repeated for alumina and barium titanate with dispersant in Fig. 3.13g-h and i-j, respectively. From the results it was shown that the dispersant did not change the direction of the particle motion. This

is somewhat expected since while the dispersant does increase the suspension conductivity as seen in Table 3.1, it also increases the surface conductivity of the particles. This means that the overall difference in conductivity between the medium and the particles should stay relatively similar. The dispersant made the effect of the non-uniform electric field more apparent as the ceramic chains attaching to the tip of the pointed electrode was able to be clearly observed. These experiments were also repeated for 250 kHz, 500 kHz and 750 kHz as well, but no changes were observed in the particle direction. Since there is only a 1 magnitude difference between 1 MHz and 100 kHz it was unlikely that there would be a change in DEP direction in this range; however, it is still possible that one could occur outside this range. Any change outside this range is outside the scope of this study due to chains having difficultly forming at the lower frequencies. Based on the above experiments, it was concluded that in the experiments where AC field was applied through two identical coplanar plate electrodes, all particles exhibited n-DEP at all tested conditions indicating that n-DEP mechanisms were present in the formation of chains in uniform electric field.

3.7 Conclusions

This study revealed assembly of Al2O3 particles in aqueous media subject to high frequency AC field for both coarse and fine particles. Formation of chains of particles due to inter-particle interactions occurred, and chain length increased with field strength and duration for both barium titanate and alumina at a similar rate. Particle differences, frequency changes, and the addition of dispersant were also explored during the work to better understand their effect on particle interactions in AC field. From these experiments it was found that while chain lengths were relatively similar between alumina and barium titanate the barium titanate particles were shown to form thicker chains with larger spaces between the chains, most likely as a result of

having greater dielectric properties. In cases for both particle types, it was shown that the decrease of the frequency had a negative impact on the formation of chains, as the fluid motion that resulted from the lower frequencies made it harder for the particles to hold together in chains. The effect of dispersant was also explored, as it has relevancy to colloidal processing such as ice-templating using AC field where dispersant is needed to make stable suspensions. In these experiments it was found that the addition of dispersant greatly improved the particles' ability to form chains. This is most likely a result of them having much greater freedom of motion within the more stable suspension. The particles being more evenly distributed throughout the suspension resulted in particles being closer to one another making it easier for them to have particle interactions with one another to form chains. It was confirmed that suspension microstructure was disrupted as soon as the field was removed, and higher field duration was associated with an improved pattern retention following the field removal. To prevent this, binder was added to suspensions so that chains could be preserved for study under SEM to confirm observations from the optical microscope.

In a deliberately created spatially non-uniform AC field, coarse particles moved toward the regions of weaker field strength (negative-DEP), whereas fine particles migrated toward the regions of stronger field strength (positive-DEP). Thus, different mechanisms were responsible for chain formation for coarse and fine particles. However, amongst finer particles there was no difference in the mechanism of formation between barium titanate and alumina particles of the same size. Furthermore, dispersant and frequencies from 250 kHz to 1 MHz did not influence the preferred response direction in the uneven electric field condition although lower frequencies still resulted in fluid motion. The current research findings help to expand the understanding of the interactions between AC field and ceramic particles in aqueous media for assembly of chains. This

research has further applications for field assisted ice-templating and in understanding the mechanisms by which discoveries in that field have been able to produce promising results in improving and tailoring the properties of ice-templated ceramics.

CHAPTER 4

CONCLUSION AND FUTURE WORK

4.1 Conclusions

In this work Al_2O_3 and $BaTiO_3$ particles in aqueous media were subject to high frequency AC field. Dielectric forces from the AC current resulted in inter-particle interactions forming chains in the direction of the field which increased in length with field strength and duration. At application of AC electric field, it could be observed that particles would rotate such that dipole interactions within the particles would align them with the AC electric field. From there a two-step process was developed in which the inter-particle interactions caused by DEP would result in self-assembly of long chains of particles. First, individual particles were attracted toward each other's dipoles which caused them to form small chains touching dipole to dipole oriented along the direction of the field. Then, the small chains developed interconnections and moved toward one another, resulting in the formation of longer chains. These interactions between particles were shown to be strongly influenced by time and voltage. Furthermore, the work showed that the particle size influenced the "suspension microstructure", where decreasing inter-particle distance in fine particle suspension caused favorable conditions for assembly. These size effects are interesting because they go against what is expected based solely on calculations of dielectric force on the particles showing that inter-particle interactions are more important for the formation of chains than simply dielectric force.

Particle property differences, frequency changes, and the addition of dispersant were also explored to better understand their effects on particle interactions in AC electric field. From these experiments it was observed that while chain lengths were relatively similar between alumina and barium titanate the barium titanate particles were shown to form thicker chains with larger spaces between the chains. This difference in chain formation was most likely as a result of barium titanate having greater dielectric properties. The findings support that while chain length was not greatly affected, particles with greater dielectric properties exhibit an increase in chaining effects as barium titanate. As was observed with the coarse alumina particles, chains that initially form group together to form larger chains over time. Therefore, from the observations it can be shown that chain to chain interactions are greater in barium titanate compared to alumina. In cases for both particle types, it was shown that the decrease of the frequency had a negative impact on the formation of chains as the fluid motion that resulted from the lower frequencies made it harder for the particles to hold together in chains.

Finally, the effect of dispersant was also explored as it has particular relevancy to colloidal processing such as ice-templating using AC electric field where dispersant is needed to make stable suspensions. In these experiments it was found that the addition of dispersant greatly improved the particles' ability to form chains. This is most likely a result of them having much greater freedom of motion within the more stable suspension. The particles being more evenly distributed throughout the suspension resulted in particles being closer to one another making it easier for them to have particle interactions with one another to form chains. It was confirmed that suspension microstructure was disrupted as soon as the AC electric field was removed, and higher field duration was associated with an improved pattern retention following the field removal. To prevent this, binder was added to suspensions so that chains could be preserved for study under

SEM to confirm observations from an optical microscope. From SEM images the optical microscope observations were able to be confirmed. It was clearly visible in SEM images that barium titanate was forming larger thicker chains that had greater inter-chain distances between them.

In a deliberately created spatially non-uniform AC field, coarse particles moved toward the regions of weaker field strength (negative-DEP), whereas fine particles migrated toward the regions of stronger field strength (positive-DEP). Thus, different mechanisms were responsible for chain formation for coarse and fine particles. However, amongst finer particles there was no difference in the mechanism of formation between barium titanate and alumina particles of the same size. Furthermore, dispersant and frequencies from 250 kHz to 1 MHz did not influence the preferred response direction in the uneven electric field conditions although lower frequencies still resulted in fluid motion. The current research findings help to expand the understanding of the interactions between AC electric field and ceramic particles in aqueous media for assembly of chains. This research has further applications for the study of field assisted ice-templating and in understanding the mechanisms by which AC electric fields can interact with ice-templated microstructures before the freezing process.

4.2 Future work

Future work for this project rests both in expanding the range of the variable conditions used in the work as well as applying it to more practical and functional designs. The limiting factors for this work thus far have been the field strength and upper and lower bounds of the frequency. While it was observed that lower frequencies are likely not ideal for forming chains, a preferential frequency for chain formation has not been explored. Furthermore, since it was

observed that lower frequencies lead to non-ideal conditions for chain formation it begs the question as to whether increasing the frequency might lead to more ideal chain formation conditions. For all experiments the gap length remained constant which may have limited the observable difference in the upper bounds of chain length. Therefore, it might be beneficial to the understanding of chain length to increase the gap size so that chain formation might be better understood. Gap size is also a consideration when applying this research to future applications. In many applications a larger size is likely to be required, particularly in freeze casting. Therefore, it is important for future work to consider increasing gap size to one that would be applicable for applications such as freeze casting so that this work might be better compared to those works.

Additionally, this work purely focused on the motion of chains in a flat plane along the glass between the electrodes. This had the benefit of not involving gravity effects in the formation of chains, but it is important to understand how the formation of chains and the motion of particles might occur in a vertical environment. Expanding the scope of this work the gap between this fundamental work and application might lead to a better understanding of the mechanisms at work. This can help build a model of understanding that can bring this research into commercial and practical use in tailoring the motion of particles and suspension microstructure of colloidal suspensions.

REFERENCES

1. R. B. Heimann "Classic and advanced ceramics: from fundamentals to applications". *John Wiley & Sons*. (2010).

2. A. G. Evans Structural reliability: a processing-dependent phenomenon. *Journal of the American Ceramic Society*, 65(3), 127-137. (1982).

3. L. Bergstrom Colloidal processing of ceramics. *Handbook of Applied Surface and Colloid Chemistry*, 1, 201-217. (2001).

4. S. Deville, Freeze-casting of porous ceramics: A review of current achievements and issues, *Adv. Eng. Mater.* 10 155–169. (2008)

5. S. Deville, A meta-analysis of the mechanical properties of ice-templated, *Ceramics and Metals Science and Technology of Advanced Materials* 16(4) (2015)

6. S. Deville, The lure of ice-templating: Recent trends and opportunities for porous materials, *Scripta Materialia*, 147 [1] 119-124 (2018).

7. H. Le Ferrand, "External fields for the fabrication of highly mineralized hierarchical architectures," *Journal of Materials Research,* 34[1] 169-93 (2019).

8. P. Niksiar, F. Y. Su, M. B. Frank, T. A. Ogden, S. E. Naleway, M. A. Meyers, J. McKittrick, and M. M. Porter, "External field assisted freeze casting," *Ceramics*, 2[1] 208-34 (2019).

9. R. M. Erb, J. J. Martin, R. Soheilian, C. Pan, and J. R. Barber, "Actuating soft matter with magnetic torque," *Advanced Functional Materials,* 26[22] 3859-80 (2016).

10. A. F. Demirörs, P. P. Pillai, B. Kowalczyk, and B. A. Grzybowski, "Colloidal assembly directed by virtual magnetic moulds," *Nature,* 503[7474] 99-103 (2013).

11. T. Schwarz, G. Petit-Pierre, and J. Dual, "Rotation of non-spherical micro-particles by amplitude modulation of superimposed orthogonal ultrasonic modes," *The Journal of the Acoustical Society of America,* 133[3] 1260-68 (2013).

12. A. Garbin, I. Leibacher, P. Hahn, H. Le Ferrand, A. Studart, and J. Dual, "Acoustophoresis of disk-shaped microparticles: A numerical and experimental study of acoustic radiation forces and torques," *The Journal of the Acoustical Society of America,* 138[5] 2759-69 (2015).

13. O. D. Velev, S. Gangwal, and D. N. Petsev, "Particle-localized AC and DC manipulation and electrokinetics," *Annual Reports Section" C"(Physical Chemistry),* 105 213-46 (2009).

14. E. V. Yakovlev, K. A. Komarov, K. I. Zaytsev, N. P. Kryuchkov, K. I. Koshelev, A. K. Zotov, D. A. Shelestov, V. L. Tolstoguzov, V. N. Kurlov, and A. V. Ivlev, "Tunable two-dimensional assembly of colloidal particles in rotating electric fields," *Scientific reports,* 7[1] 1-10 (2017).

15. R. Pethig, "Dielectrophoresis: Status of the theory, technology, and applications," *Biomicrofluidics,* 4[2] 022811 (2010).

16. C. Siebman, O. D. Velev, and V. I. Slaveykova, "Alternating current-dielectrophoresis collection and chaining of phytoplankton on chip: Comparison of individual species and artificial communities," *Biosensors,* 7[1] 4 (2017).

17. A. Boccaccini, C. Kaya, and K. Chawla, "Use of electrophoretic deposition in the processing of fibre reinforced ceramic and glass matrix composites: a review," *Composites Part A: Applied science and manufacturing,* 32[8] 997-1006 (2001).

18. P. Sarkar and P. S. Nicholson, "Electrophoretic deposition (EPD): mechanisms, kinetics, and application to ceramics," *Journal of the American Ceramic Society,* 79[8] 1987-2002 (1996).

19. O. D. Velev and K. H. Bhatt, "On-chip micromanipulation and assembly of colloidal particles by electric fields," *Soft Matter,* 2[9] 738-50 (2006).

20. Y.-H. Su, M. Tsegaye, W. Varhue, K.-T. Liao, L. S. Abebe, J. A. Smith, R. L. Guerrant, and N. S. Swami, "Quantitative dielectrophoretic tracking for characterization and separation of persistent subpopulations of Cryptosporidium parvum," *Analyst,* 139[1] 66-73 (2014).

21. J. Cottet, O. Fabregue, C. Berger, F. Buret, P. Renaud, and M. Frénéa-Robin, "MyDEP: a new computational tool for dielectric modeling of particles and cells," *Biophysical journal,* 116[1] 12-18 (2019).

22. S. Afshar, E. Salimi, K. Braasch, M. Butler, D. J. Thomson, and G. E. Bridges, "Multi-frequency DEP cytometer employing a microwave sensor for dielectric analysis of single cells," *IEEE Transactions on Microwave Theory and Techniques,* 64[3] 991-98 (2016).

23. S. Ghashghaie, E. Marzbanrad, B. Raissi, C. Zamani, and R. Riahifar, "Effect of low frequency electric field parameters on chain formation of ZnO nanoparticles for gas sensing applications," *Journal of the American Ceramic Society,* 95[6] 1843-50 (2012).

24. Y. Ai, Z. Zeng, and S. Qian, "Direct numerical simulation of AC dielectrophoretic particle–particle interactive motions," *Journal of colloid and interface science,* 417 72-79 (2014).

25. Y. Ai and S. Qian, "DC dielectrophoretic particle–particle interactions and their relative motions," *Journal of colloid and interface science,* 346[2] 448-54 (2010).

26. S. "Akurati, S Qian, D. Ghosh, "AC electric field-assisted fabrication of ice-templated alumina materials and remarkable enhancement of compressive strength", *Scripta Materialia,* 206 [1] (2022)

27. Barsoum, M. W. "Fundamentals of ceramics." *CRC press*. (2019).

28. Auerkari, P. "Mechanical and physical properties of engineering alumina ceramics." Espoo: *Technical Research Centre of Finland.* (Vol. 23) (1996).

29. Nowotny, J., & Rekas, M. "Positive temperature coefficient of resistivity for $BaTiO_3$-based materials." *Ceramics international*, 17(4), 227-241. (1991).

30. Wu, L., Chure, M. C., Wu, K. K., Chang, W. C., Yang, M. J., Liu, W. K., & Wu, M. J. "Dielectric properties of barium titanate ceramics with different materials powder size." C*eramics International*, 35(3), 957-960. (2009).

31. S. Deville, E. Maire, A. Lasalle, A. Bogner, C. Gauthier, J. Leloup, and C. Guizard, "Influence of particle size on ice nucleation and growth during the ice-templating process," *Journal of the American Ceramic Society*, 93[9] 2507-10 (2010).

32. Q. Chen and Y. J. Yuan, "A review of polystyrene bead manipulation by dielectrophoresis," *RSC advances*, 9[9] 4963-81 (2019).

33. D. Zhao, R. Liu, C. Luo, Y. Guo, C. Hou, Q. Zhang, Y. Li, W. Jia, and H. Wang, "Dielectrophoretic Assembly of Carbon Nanotube Chains in Aqueous Solution," *Advanced Fiber Materials*, 3[5] 312-20 (2021).

34. K. K. Sarojini, S. V. Manoj, P. K. Singh, T. Pradeep, and S. K. Das, "Electrical conductivity of ceramic and metallic nanofluids," *Colloids and Surfaces A: Physicochemical and Engineering Aspects*, 417 39-46 (2013).

35. I. Zakaria, W. Azmi, W. Mohamed, R. Mamat, and G. Najafi, "Experimental investigation of thermal conductivity and electrical conductivity of Al_2O_3 nanofluid in water-ethylene glycol mixture for proton exchange membrane fuel cell application," *International Communications in Heat and Mass Transfer*, 61 61-68 (2015).

32. N. Bharath Gundrati, "Modeling Interactions in Concentrated Ceramic Suspensions Under AC Electric Field," (2021).

Appendix A
SUPPLEMENTAL FIGURE

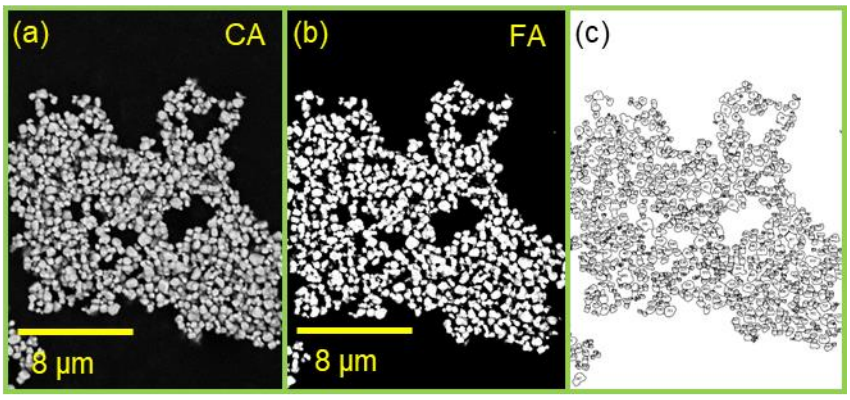

Fig.S1 (a) SEM image of the powder (b) is the image after sharpening and increasing contrast. (c) is the image of the particle outlines after particle analysis

VITA

James E. John IV was born in Charlottsville VA, on September 1st, 1996. He graduated from Old Dominion University in 2019 with a Bachelor of Engineering degree in Mechanical Engineering. Following his graduation, he was accepted into the Old Dominion University graduated program for mechanical engineering and worked with Dr. Dipankar Ghosh in his LEEM laboratory.

John, J., Qian, S., Ghosh D., (2022) "Assembly of alumina particles in aqueous suspensions induced by high-frequency AC electric field" Journal of the American Ceramic Society (Accepted)

John, J., Parai, R., Akurati, S., Ghosh D., Novel Processing of Directionally Porous Sintered Barium Titanite Ceramics. 44th International Conference on Advanced Ceramics and Composites, 9th Global Young Investigator Forum, Daytona Beach FL, USA, January 26-31, 2020. (Oral)

Ghosh, D., Banda, M., John, J., Terrones, D.A., (2018)" Dynamic strength enhancement and strain rate sensitivity in ice-templated ceramics processed with and without anisometric particles." Scripta Materialia.154, pp 236-240